Title: Endothelial vacuole membrane enriched aquaporins regulate microvascular lumenization in development and hyperglycemia

Changsheng Chen[1, *], Yinyin Qin[1, 2, *], Yidan Xu[3, 4, *], Lixun Chen[3, 4], Linnong Wang[3, 4], Dong Liu[1, #]

[1] School of Life Sciences, Nantong Laboratory of Development and Diseases; Second Affiliated Hospital; Key Laboratory of Neuroregeneration of Jiangsu and Ministry of Education, Co-innovation Center of Neuroregeneration, Nantong University, Nantong, China

[2] Suzhou Science & Technology Town Hospital, Suzhou, China

[3] Department of Ophthalmology, Nanjing First Hospital, Nanjing Medical University, Nanjing, China.

[4] Nanjing Red Cross Eye Bank, Nanjing, China.

*, these authors contributed equally to this work

#, author for correspondence

Contact details for Correspondence:

Dong Liu , Ph.D

Nantong Laboratory of Development and Diseases, Nantong University

Qixiu Road 19, Nantong, China, 226001

Phone: + (86) - 18605133927

Fax: + (86)-513-85012809

Email: liudongtom@gmail.com; tom@ntu.edu.cn

Abstract

In patients with diabetic microvascular complications, reduced vessel perfusion or vascular occlusion is a common characteristic which will cause the insufficient blood supply. However, identification of novel regulators involved in microvascular lumenization defects is hindered by the lacking of a model for imaging the blood vessels at high resolution *in vivo*. Taking advantage of the transparency of zebrafish, we observed the reduction of vascular diameter and compromised perfusion in high glucose treated embryos. RNA sequencing and whole-mount *in situ* hybridization analysis indicated that two aquaporins (*aqp1a.1* and *aqp8a.1*) were significant down-regulated, which was further confirmed by endothelial specific Q-PCR. It was also shown that the two aqps were spatio-temporally enriched in the endothelial cells (ECs) of vascular system. Zebrafish with loss of *aqp1a.1* or *aqp8a.1* displayed lumenization defects in intersegmental vessels, recapitulating the phenotype in hyperglycemic zebrafish model. While overexpressing the aquaporins in zebrafish promoted the enlargement of the vascular diameter. Moreover, the defective vasculature induced by high-glucose treatment could be rescued by *aqp1a.1* upregulation. In addition, both *aqp1a.1* and *apq8a.1* were localized in the intracellular vacuoles in cultured ECs as well as in the ECs of sprouting ISVs, and loss of Aqps caused the reduction of those vacuoles, which was required for lumenization. Finally, we found that the expression of human *AQP1* was downregulated in diabetic human retina samples and high-glucose treated human retinal microvascular endothelial cells. All these results suggest that EC-enriched aquaporins have a role in developmental and pathological blood vessel lumenization, and they might be potential targets for gene therapy to cure diabetes-related vascular lumenization defects.

Key words: diabetic retinopathy; Aquaporin; lumenization; rescue

Introduction

Hyperglycemia caused microvascular complications, including hemorrhages, microaneurysms, capillary non-perfusion, and neovascularization (Agemy et al., 2015; Beckman and Creager, 2016; Duh et al., 2017; Toh et al., 2019; Wang and Lo, 2018), are the major source of morbidity and mortality in diabetes. However, it remains unclear how does the reduced perfusion of blood vessels form under hyperglycemic conditions. To address this, the zebrafish (*Danio Rerio*) model was utilized in our study, which offers superior properties in cardiovascular research (Gore et al., 2012; Liu and Stainier, 2012). The transparency of zebrafish embryos allows to perform high-resolution imaging analysis of vascular development *in vivo*. Importantly, the zebrafish can live up to the first week of development without a functional vasculature, allowing a detailed analysis even in animals with severe cardiovascular defects; by contrast, avian and mammalian embryos die rapidly in the absence of a functional cardiovascular system. Moreover, a variety of established zebrafish diabetes mellitus (DM) models are available and easy to manipulate (Chen and Liu, 2022).

Aquaporin (AQPs) are a superfamily of tetrameric membrane proteins that involve in transportation of water across cell plasma membranes (Papadopoulos et al., 2008; Smith and Agre, 1991). Several of these small, integral membrane proteins are also known for transfer of other small, uncharged solutes (e.g. glycerol), to maintain fluid homeostasis (Verkman, 2005). Accumulating evidences suggest that specific classes of AQPs are involved in angiogenesis and endothelial cell (EC) function under physiological and pathological conditions (Ribatti et al., 2014; Verkman, 2002). In current work, the zebrafish embryos were immersed into a high glucose solution to mimic a hyperglycemic state. Under the treatment, the narrowed and reduced perfusion of blood vessels in both eyes and trunks of zebrafish embryos were observed. It has been revealed that two endothelial enriched aquaporins, *aqp1a.1* and *aqp8a.1*, were significantly down-regulated upon high glucose treatment. These results suggest a role of aquaporins in both developmental and hyperglycemic blood vessels. Here, we found that *apq1a.1* or *aqp8a.1* loss-of-function led to the reduction of diameter and perfusion

of intersegmental vessels, which recapitulated the vascular phenotype of hyperglycemic zebrafish embryos. However, gain-of-function of *apq1a.1* or *aqp8a.1* in zebrafish embryos caused the increased diameter of blood vessels. Moreover, overexpression of *apq1a.1* in hyperglycemic zebrafish embryos rescued the defective vascular phenotype. In addition, gene expression analysis of retina samples from 49 non-diabetic and 54 diabetic donors showed that the human AQP1 (orthologous to zebrafish *aqp1a.1*) was also down-regulated under diabetic condition and high-glucose treated human retinal microvascular endothelial cells. All taken together, AQPs are important regulators in blood vessel lumenization during vascular system development and hyperglycemia.

Results

Hyperglycemia leads to vascular lumenization defect in zebrafish during embryogenesis

To examine the effects of high glucose on vascular development, a hyperglycemia zebrafish model was established using the transgenic line *Tg(fli1ep:EGFP-CAAX)*^{ntu666}, in which an endothelial enhancer/promoter fragment (fli1ep) was employed to drive the specific expression of the enhanced green fluorescent protein (EGFP) in ECs, and the CAAX membrane targeting motif was able to guarantee the localization of EGFP at the surface of ECs (Fig.S1). In this line, a direct non-invasive visualization of the zebrafish vasculature can be achieved under a conventional fluorescence microscopy or a confocal microscopy. A hyperglycemic state in zebrafish embryos was achieved by immersing them into a high glucose solution from 2 days post fertilization (dpf), and fluorescence imaging of the vasculature was performed at 3 dpf (Fig.1A and S2). The high glucose treatment did not yield phenotypically differences and developmental defects on zebrafish embryos, but the vasculature was substantially influenced. Under this condition, the vessel diameters were significantly decreased compared with the untreated control counterparts, including the inner optic circle (IOC) in the eyes as well as the intersegmental vessels (ISVs), dorsal aorta (DA) and posterior cardinal vein (PCV) in the trunk (Fig.1B-C'' and Fig.1E-F''). The IOC in zebrafish eyes and the ISVs in zebrafish trunk were declined by 27.9% and 36.8%, respectively (Fig.1D and H). Also,

microangiography analysis revealed that 59% of the narrowed ISVs were not perfused based on a (Fig.1G), suggesting that the dysfunctional vascular lumens were formed after high glucose induction.

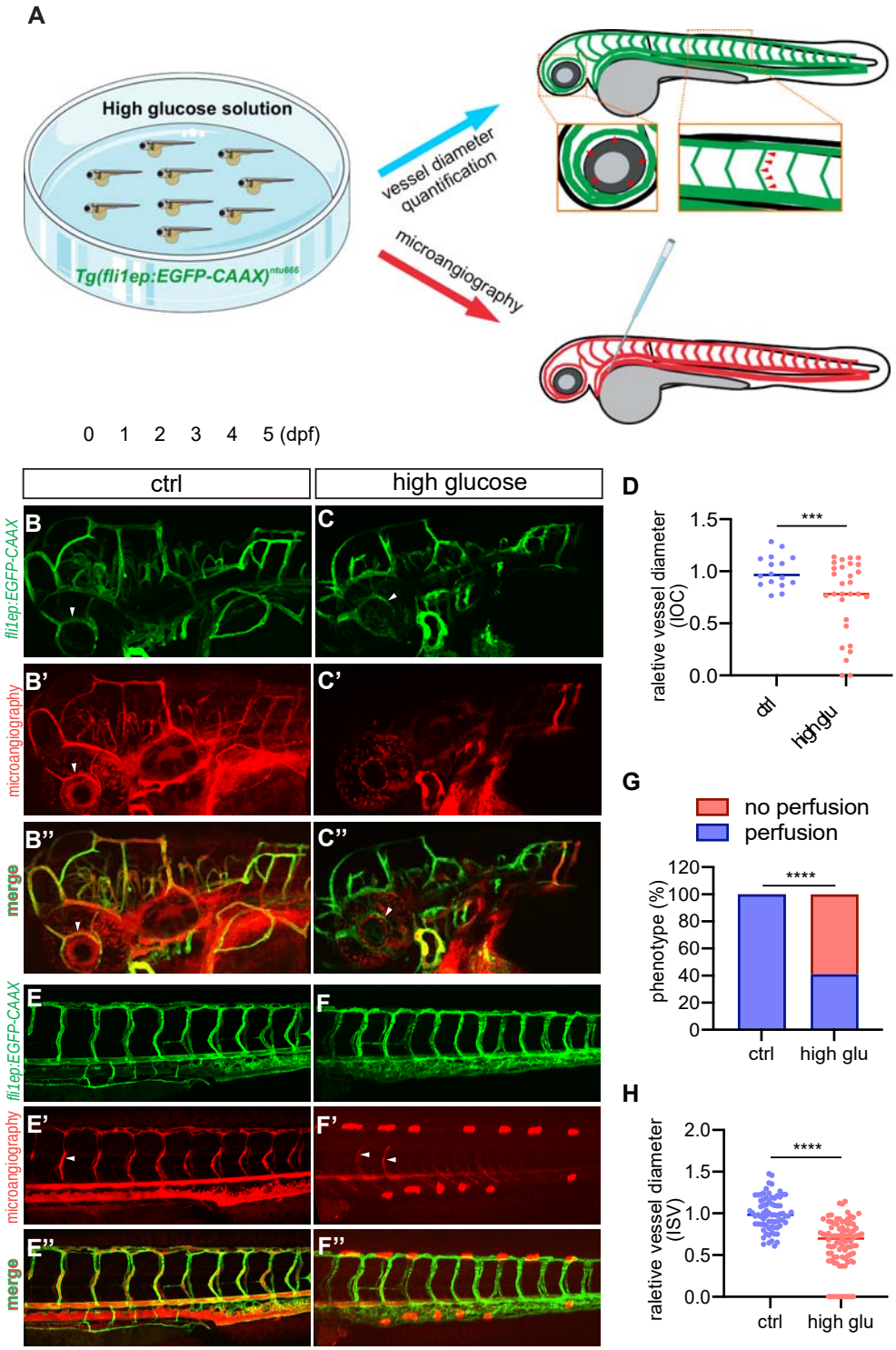

Figure 1. High glucose treatment affects vascular lumenization in zebrafish embryos. A, Schematic representation of establishing zebrafish hyperglycemia/DM model. Zebrafish embryos are immersed into high glucose solution from 2 to 3 dpf. Microangiography and confocal imaging are performed afterwards. **B-C'',** Representative confocal images of IOC phenotypes in 3-dpf *Tg(fli1ep:EGFP-CAAX)*^{ntu666} transgenic line with or without glucose treatment. White arrowheads indicate the IOC. **D,** Quantification of IOC diameter. **E-F'',** Representative confocal images of ISV phenotypes in 3-dpf *Tg(fli1ep:EGFP-CAAX)*^{ntu666} transgenic line with or without glucose treatment. White arrowheads indicate the ISV. **G,** The incidence of normal and non-perfused ISVs in 3-dpf *Tg(fli1ep:EGFP-CAAX)*^{ntu666} transgenic line with or without glucose treatment. **H,** Quantification of ISV diameter. Data are shown as mean ± s.e.m. A two-tailed, unpaired Student's t-test is applied. ***, $p < 0.001$. ****, $p < 0.0001$.

High glucose treatment caused the downregulation of expression of *aqp1a.1* and *aqp8a.1*

To further explore which genes are altered upon glucose treatment, transcriptome sequencing analysis was performed. Compared to those in control zebrafish, the expression of a serials of genes were significantly altered in 72 and 96 hours post fertilization (hpf) embryos treated with high glucose, with 642 genes upregulated and 1,149 genes downregulated at 72 hpf, as well as 1,259 genes upregulated and 1,851 genes downregulated at 96 hpf (Fig.2A and B). Approximately 30% of the upregulated genes and 40% of the downregulated genes were overlapped between 72 and 96 hpf (Fig.2C). KEGG analysis revealed that a variety of biological processes or signaling pathways related to glucose and lipid metabolism, immune responses and vascular regulation, were enriched in embryos under hyperglycemic condition (Fig.2D). Several EC-enriched genes, like *cxcr4a* and *esm1*, were found to be upregulated after high glucose treatment, while the aquaporins (*aqp1a.1* and *aqp8a.1*) exhibited reduced expressions (Fig.2E and F). Further whole-mount ISH assay demonstrated that the zebrafish *aqp1a.1* and *aqp8a.1* were highly enriched in ECs of vascular system (Fig.S3). Additionally, the expressions of *aqp1a.1* and *aqp8a.1* in hyperglycemic zebrafishes were validated by real-time qPCR and ISH assay, and the results were consistent with the transcriptomic data (Fig.3A-H). To further examine whether *aqp1a.1* and *aqp8a.1*

were down-regulated in ECs of high glucose treated embryos, we performed qPCR assay with isolated ECs. The ECs in control and high glucose-treated group at 96 hpf were respectively sorted by FACs and subsequently used for RNA isolation (Fig.3I). Upon high glucose induction, both *aqp1a.1* and *aqp8a.1* in ECs were significantly downregulated (Fig.3J and K).

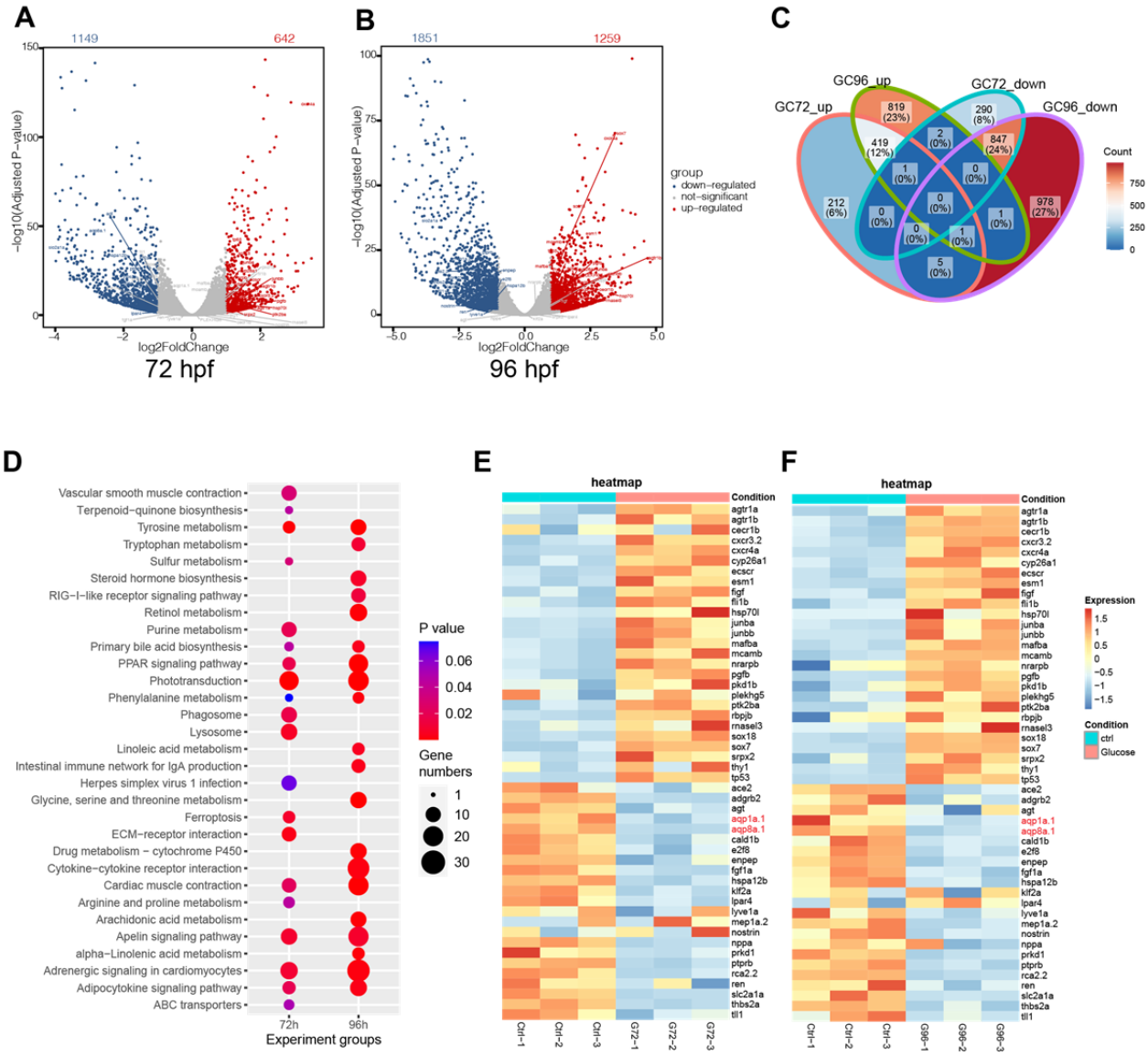

Figure 2. Transcriptomic profiling of *Tg(fli1ep:EGFP-CAAX)^{ntu666}* transgenic line with or without glucose treatment. A and B, Volcano plots of downregulated genes (blue dots), upregulated genes (red dots), and unchanged genes (grey dots) in high glucose-treated group versus the control group at 72 and 96 hpf, respectively. **C,** Venn diagram shows the overlapping upregulated and downregulated DEGs upon high glucose treatment at 72 and 96 hpf. **D,** KEGG

enrichment analysis reveals the signaling pathways and the cellular and biological processes that the DEGs are involved. **E and F,** Heatmaps based on RNA-seq data demonstrate that *aqp1a.1* and *aqp8a.1* are downregulated upon high glucose treatment.

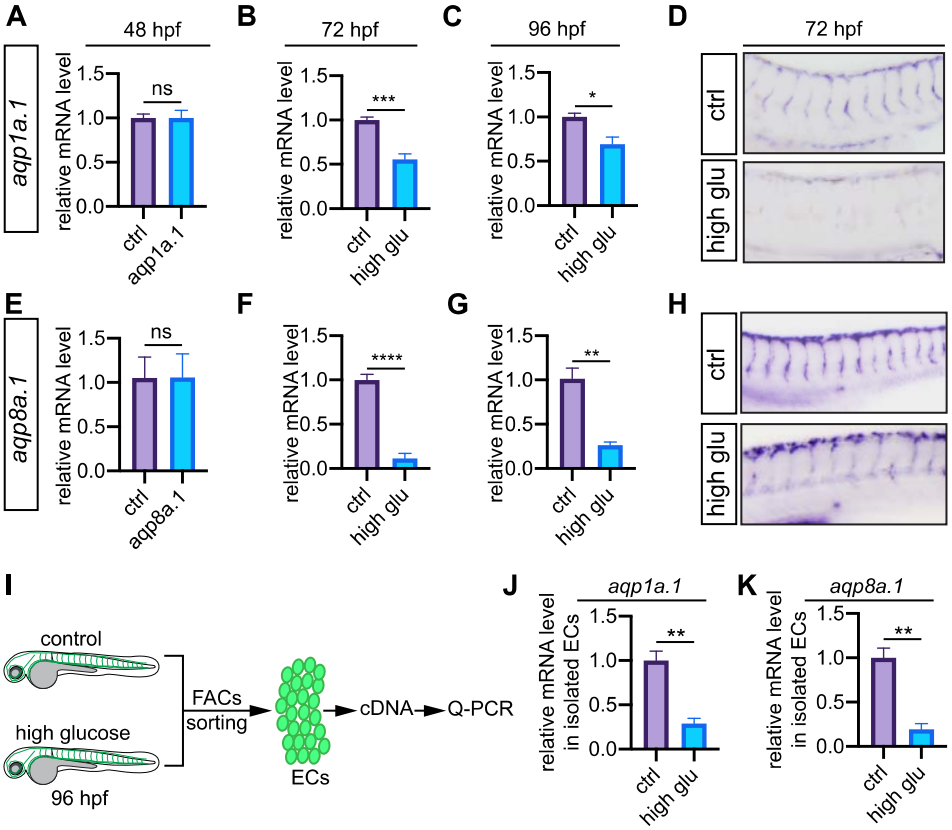

Figure 3. Zebrafish *aqp1a.1* and *aqp8a.1* are differentially expressed upon high glucose treatment. A-H, Expressions of *aqp1a.1* and *aqp8a.1* in zebrafish after high glucose treatment are examined by Q-PCR and ISH. **I,** Schematic representation of isolation of ECs from control and high glucose-treated *Tg(kdrl:EGFP)* zebrafish embryos for RNA extraction and Q-PCR. **J and K,** Quantification of *aqp1a.1* and *aqp8a.1* expressions in isolated ECs. Data are shown as mean ± s.e.m. A two-tailed, unpaired Student's t-test is applied. **, $p < 0.01$.

aqp1a.1 or *aqp8a.1* are essential for blood vessel lumenization

To gain an insight into the functions of EC-expressed AQPs in vascular system, we performed gene functional analysis using zebrafish model. We first used CRISPR/Cas9 genome editing method to knockout either *aqp1a.1* or *aqp8a.1* in *Tg(fli1ep:EGFP-*

172 *CAAX)*^{ntu666} transgenic zebrafish (Fig.S4 and S5). Homozygous *aqp1a.1*-knockout
173 mutants displayed reduced lumen size of the small intersegmental vessels (ISVs),
174 which were generated from angiogenesis. However, the diameters of large vessels,
175 including dorsal aortae (DA) and posterior cardinal vein (PCV), which are generated
176 through vasculogenesis, were not significantly affected (Fig.4A). Upon *apq1a.1* gene
177 deletion, the diameters of DV and PCV only decreased by 4.2% and 4.7% at 48 hpf,
178 respectively, whereas the average diameter of ISVs showed an approximately 20%
179 decrease (Fig.4B). To examine whether the vascular defects were caused by off-target
180 effects of the CRISPR system, we knocked down *aqp1a.1* expression by injecting the
181 *aqp1a.1* splicing morpholino into *Tg(fli1ep:EGFP-CAAX)*^{ntu666} embryos. The vascular
182 defects were recapitulated and even enhanced within *aqp1a.1*-MO-injected zebrafish
183 embryos (Fig.S6). In addition, the injection of *aqp1a.1* mRNA rescued the vascular
184 defects in *aqp1a.1* morphants. These results suggested that Aqp1a.1 exerted a role in
185 regulation of vascular lumenization. However, the homozygous or even heterozygous
186 *aqp8a.1*-knockout mutants have not been obtained since all harvested embryos were
187 genotyped as multiples of 3 base pairs deletion (Fig.S5). We were of the opinion that
188 targeted deletion of the *aqp8a.1* gene resulted in embryonic lethality in zebrafish.
189 Although it was hardly to get *aqp8a.1*-knokout mutant, the G0 generation chimeras,
190 which contained the *aqp8a.1*-knockout cells, also displayed narrowed vessel lumens
191 (Fig.4A). Compared with those of control, the diameters of DA, PCV and ISVs in
192 *aqp8a.1*-KO G0 mutants decreased 11.2%, 9.8% and 13.3%, respectively (Fig. 4B). In
193 order to test whether the vascular phenotypic change was result from *aqp8a.1* loss of
194 function, we injected *aqp8a.1*-specific morpholino into *Tg(fli1ep:EGFP-CAAX)*^{ntu666}
195 embryos to block *aqp8a.1* pre-RNA splicing. The morpholino-mediated *aqp8a.1*
196 knockdown led to reduced lumen diameters of blood vessels, which mimicked the
197 phenotype caused by *aqp1a.1* loss-of-function (Fig.S6). Also, non-perfused or
198 perfusion-defective ISVs were more frequently observed in *aqp1a.1* or *aqp8a.1*
199 knockout embryos based on microangiography analysis (Fig.4C and D). All the results
200 suggested that loss-of-function of either *aqp1a.1* or *aqp8a.1* impaired the vascular
201 lumen formation during blood vessel development.

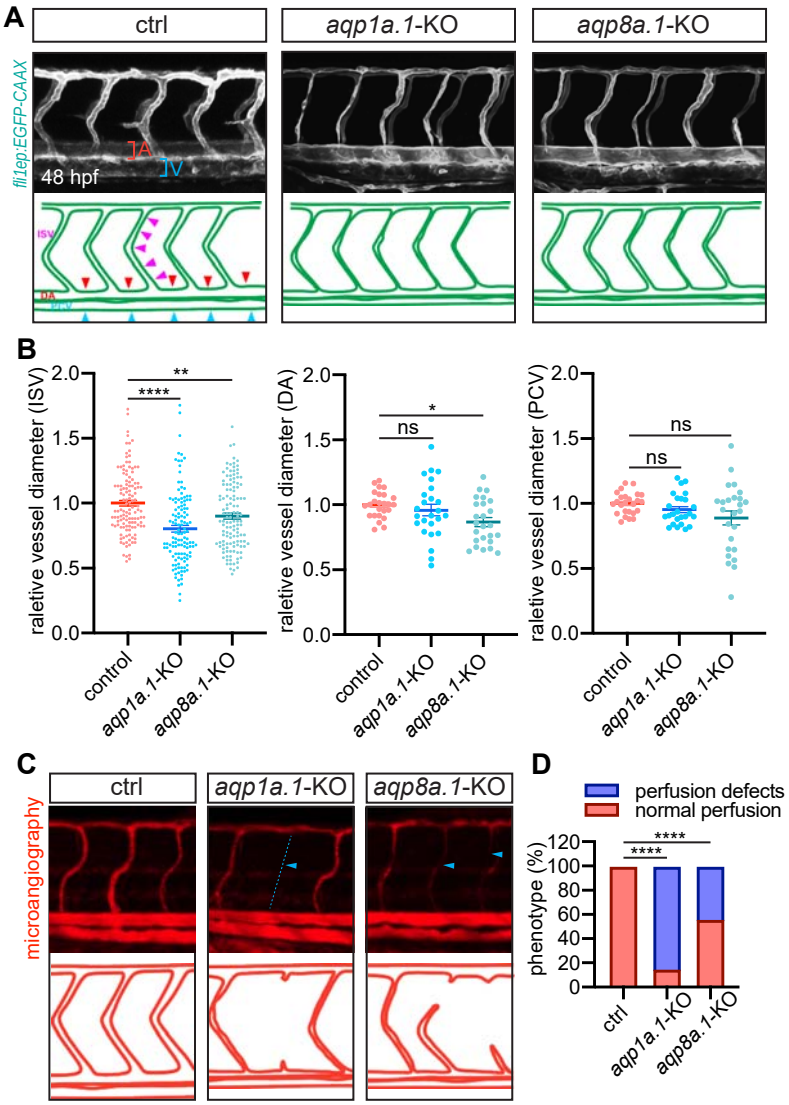

Figure 4. Knockout of EC-enriched aquaporins (*aqp1a.1* or *aqp8a.1*) leads to defective vascular lumenization in zebrafish. A, Confocal images of ISV phenotypes in 48-hpf *Tg(fli1ep:EGFP-CAAX)^{ntu666}* control embryos and *aqp1a.1*-knockout and *aqp8a.1*-knockout embryos. Red and blue square brackets indicate artery and vein, respectively. Magenta, red and blue arrowheads in the representative sketch indicate the positions for vessel diameter measurement for ISV, DA and PCV, respectively. **B,** Quantification of the diameters of ISV, DA and PCV. Data are shown as mean ± s.e.m. One-way ANOVA analysis is applied. **C,** Microangiography of the trunk region in 72-hpf *Tg(fli1ep:EGFP-CAAX)^{ntu666}* control embryos and *aqp1a.1*-knockout and *aqp8a.1*-knockout embryos. Blue arrowheads indicate the perfusion-deficient ISVs. **D,** The incidence of normal and defective perfused ISVs in 72-hpf

213 *Tg(fli1ep:EGFP-CAAX)*^{ntu666} control embryos and *aqp1a.1*-knockout and *aqp8a.1*-knockout
214 embryos. ns, not significant. *, $p<0.05$. **, $p < 0.01$. ****, $p < 0.0001$.

215

216 Next, we performed Aqp1a.1/Aqp8a.1 gain of function analysis to further confirm the
217 contribution of EC-expressed aquaporins on vascular lumenization. *Tg(fli1ep:aqp1a.1-*
218 *mCherry)*^{ntu667} and *Tg(fli1ep:aqp8a.1-EGFP)*^{ntu668} lines were constructed to overexpress
219 fluorescently-labeled Aqp1a.1 and Aqp8a.1 in zebrafish, respectively. Overexpressing
220 either of them induced the enlargement of the blood vessel lumens (Fig.5A).
221 Overexpression of *aqp1a.1* led to increases in DA and PCV diameter by 15.2% and
222 17.3%, respectively (Fig.5B and C), while the diameter of ISVs increased almost half of
223 the control (approx. 47%) upon *aqp1a.1* overexpression (Fig.5D). The morphology of
224 blood vessels in *aqp8a.1* gain of function embryos resembled the vascular phenotype of
225 *aqp1a.1* overexpression (Fig.5A). Diameters of DA, PCV, and ISVs increased 22.4%,
226 23.2% and 32.2% in *aqp8a.1* overexpressed zebrafish embryos, respectively (Fig.5B-D).
227 Moreover, co-overexpression of *aqp1a.1* and *aqp8a.1* in zebrafish endothelial cells
228 resulted in further dilation of DA, but the diameters of PCV and ISVs did not present
229 significant increase compare to single aquaporin (*aqp1a.1* or *aqp8a.1*) overexpression
230 (Fig.5A-D). The diameters of DA, PCV and ISVs in *aqp1a.1* and *aqp8a.1* co-
231 overexpressed line exhibited 30.9%, 19.8% and 39.0% elevation compared to control
232 (Fig.5A-D). These results suggested a role of Aqp1a.1 and Aqp8a.1 in promoting
233 vascular lumen formation.

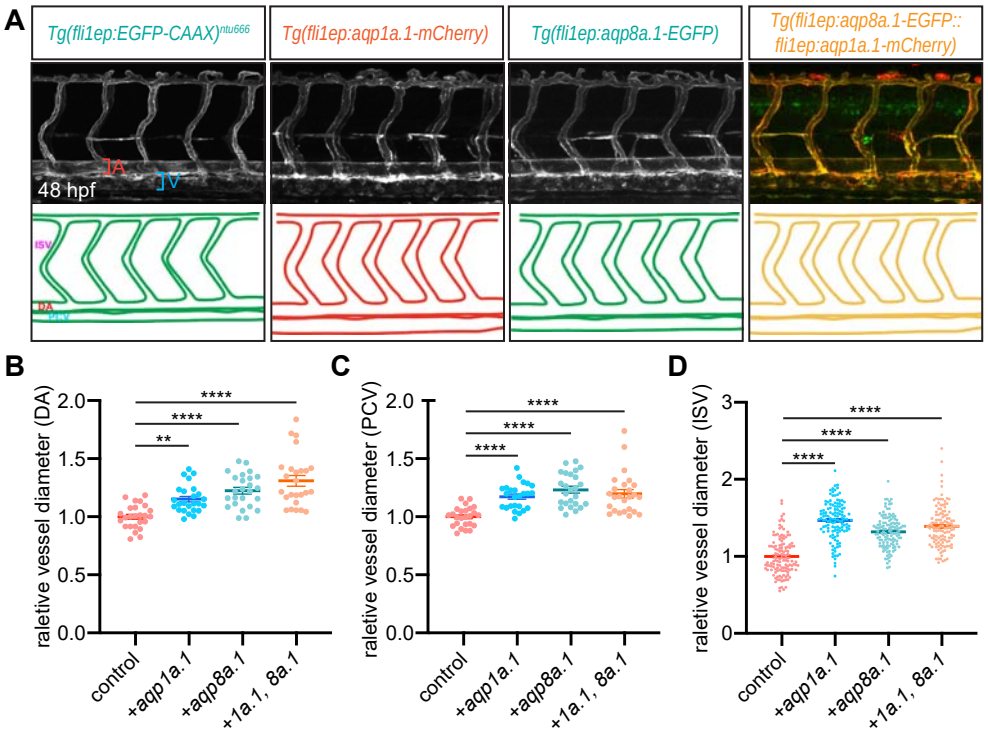

Figure 5. Overexpression of EC-enriched aquaporins (*aqp1a.1* or *aqp8a.1*) in ECs results in vessel lumen enlargement in zebrafish. A, Confocal images of ISV phenotypes in 48-hpf *Tg(fli1ep:EGFP-CAAX)*^{ntu666} transgenic line (control), *Tg(fli1ep:aqp1a.1-mCherry)*^{ntu667} transgenic line (*aqp1a.1* overexpression), *Tg(fli1ep:aqp8a.1-EGFP)*^{ntu668} transgenic line (*aqp8a.1* overexpression), and *Tg(fli1ep:aqp8a.1-EGFP::fli1ep:aqp1a.1-mCherry)* double transgenic line (*aqp1a.1* and *aqp8a.1* co-overexpression). Red and blue square brackets indicate artery and vein, respectively. **B-D,** Quantification of the diameters of ISV, DA and PCV. Data are shown as mean ± s.e.m. One-way ANOVA analysis is applied. **, $p < 0.01$. ****, $p < 0.0001$.

In addition, we applied $HgCl_2$ treatment on *Tg(fli1ep:EGFP-CAAX)*^{ntu666} zebrafish embryo to inhibit aquaporin function and check its effect on the vascular lumenization. Mercury has been commonly used to specifically block the water-channel activity of Aqp1a.1 and Aqp8a.1(Khan et al., 2013; Liu et al., 2006, p. 8; Preston et al., 1992; Yang et al., 2006). To screen the proper dosage for the treatment, we tried varied doses of $HgCl_2$. It was shown that the embryos exposed to 1.6 μM $HgCl_2$ from 22 to 48 hpf had no obvious morphological defects. Here, lower concentration (0.4 μM) of $HgCl_2$ was

252 sufficient to narrow the diameter of the blood vessels (Fig.S7). Under this concentration,
253 there were 15.4%, 15.7%, and 16.9% decreases in the diameters of DV, PCV, and ISVs,
254 respectively. With further increase in $HgCl_2$ concentration, the diameters of all the
255 aforementioned blood vessels reduced more remarkably (Fig.S7). As a result, blocking
256 the channel activity of aquaporins led to defective vascular tube formation.

257

258 **Overexpression of *aqp1a.1* rescues hyperglycemia-induced vascular**
259 **lumenization defect**

260 To elucidate whether the hyperglycemia-induced vascular lumenization defect is AQP
261 dependent, we establish a transgenic construct, in which *apq1a.1* was specifically
262 overexpressed in ECs. As shown in Fig.6A, the *pTol2-fli1ep-aqp1a.1-mCherry* plasmid
263 and Tol2 transposase mRNA were co-injected into 4-cell stage embryos of
264 *Tg(fli1ep:EGFP-CAAX)*^{ntu666} progeny. By using this strategy, the mCherry-labeled
265 Aqp1a.1 was mosaically expressed in the zebrafish vascular system. After injection, the
266 embryos were first selected for mosaic mCherry fluorescence and subsequently
267 immersed into glucose solution from 48 hpf for 24 h prior to confocal imaging analysis
268 (Fig.6B). As expected, a few ISVs exhibited both mCherry and GFP expression, and
269 these ISVs displayed wider lumens than the ones without mCherry expression (Fig.6C
270 and D). These results demonstrated that overexpression of *aqp1a.1* recovered the
271 defective lumen formation caused by hyperglycemia.

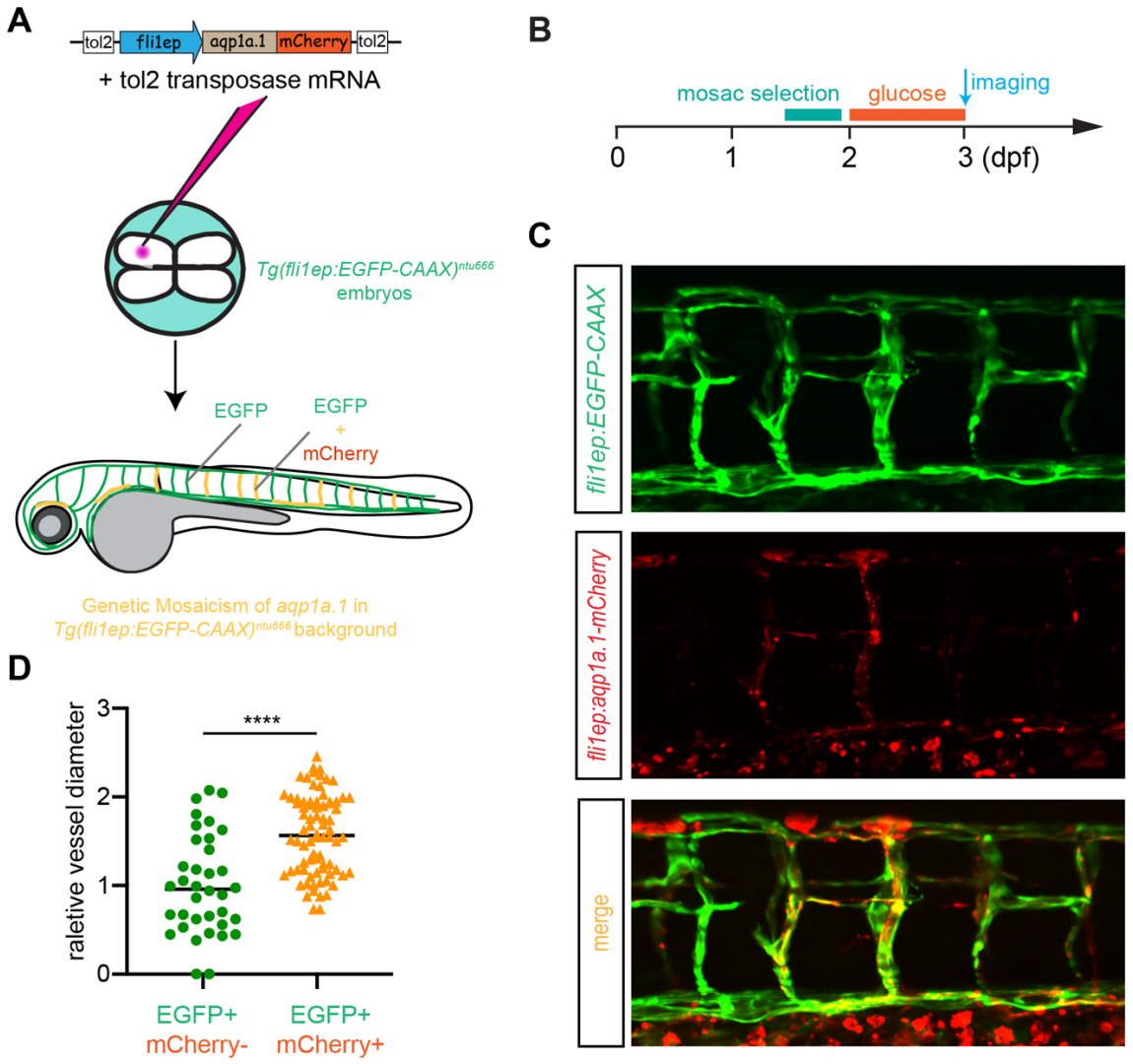

Figure 6. Overexpression of zebrafish *aqp1a.1* rescues hyperglycemia-caused defective lumenization. A, Schematic representation of establishment of *aqp1a.1*-overexpressed transgenic line under *Tg(fli1ep:EGFP-CAAX)^{ntu666}* background. DNA construct and Tol2 transposase mRNA are co-injected at 4-cell stage to establish a chimera line, in which the mCherry-labeled Aqp1a.1 is mosaically expressed in vascular system. **B,** Embryos are selected and immersed into glucose solution from 2 to 3 dpf prior to imaging. **C,** Representative confocal images of ISVs in 3-dpf *Tg(fli1ep:EGFP-CAAX::fli1ep:apq1.1-mCherry)* double transgenic line. **D,** Quantification of the lumen diameters in ISVs with or without Aqp1a.1 expression. Data are shown as mean ± s.e.m. A two-tailed, unpaired Student's t-test is applied. ****, $p < 0.0001$.

AQPs contribute to vascular lumenization through intracellular vacuoles

Given that intracellular vacuoles fusion is an essential way of vascular lumenization in zebrafish ISVs (Kamei et al., 2006), whether AQPs involves in this process is undetermined. By expressing the fluorescently-labeled *aqp1a.1* and *aqp8a.1* in human umbilical vein endothelial cells (HUVECs), we found that both Aqps were localized in the endothelial cell membrane and highly enriched in vacuoles membrane subcellularly (Fig.7A and B). Moreover, Aqp1a.1 was co-localized with Cdc42, a marker for intracytoplasmic vesicles (Kamei et al., 2006; Osmani et al., 2010), in sprouting ISVs (Fig.7C). Meanwhile, loss-of-function of *aqp1a.1* and *aqp8a.1* led to the reduction of intracellular vacuoles and defective endothelial tube assembly in ISVs (Fig.7D). In addition, the area of endothelial vacuoles was significantly declined upon loss of Aqps in endothelial cells of ISVs (Fig.7E and F). These results indicated that *aqp1a.1* and *aqp8a.1* displayed cytoplasmic vacuolar localization and required for the intracellular vacuole-mediated endothelial tube formation.

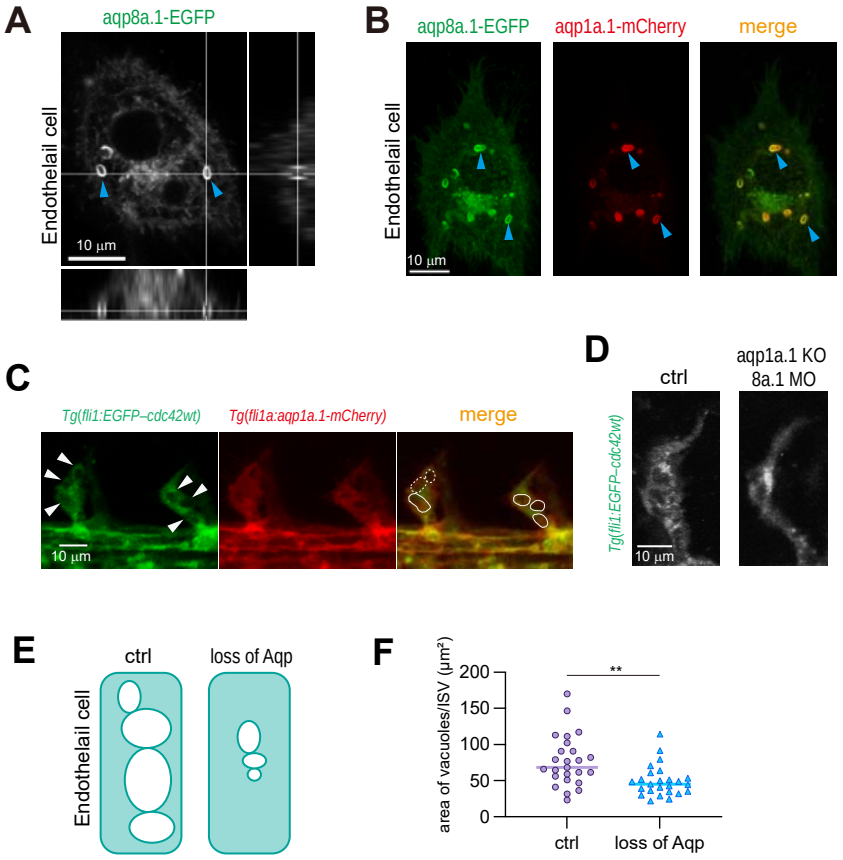

298 **Figure 7. Aqp1a.1 and Aqp8a.1 localize in intracellular vacuoles of ECs *in vitro* and *in***
299 ***vivo*. A and B,** Fluorescently-labeled Aqps are expressed on the surface of cytoplasmic
300 vacuoles (blue arrowheads) in HUVECs. **C,** Confocal imaging of zebrafish ISVs in *Tg(fli1:EGFP-*
301 *cdc42wt::fli1a:aqp1a.1-mCherry)* double transgenic line, in which the EGFP-labeled Cdc42
302 protein marks the vacuolar structures (white arrowheads) and Aqp1a.1 is labeled by mCherry.
303 Aqp1a.1 co-localizes with intracellular vacuoles (dashed circles). Scale bars, 10 μm. **D,**
304 Knockout aqp1a.1 and knockdown aqp8a.1 in zebrafish leads to defective vascular lumen
305 formation in ISVs. **E,** Schematic representation of intracellular vacuole change upon loss of Aqp.
306 **F,** Quantification of the area of intracellular vacuoles in zebrafish ISVs. Data are shown as mean
307 ± s.e.m. A two-tailed, unpaired Student's t-test is applied. **, $p < 0.01$.

308

309 **Expression of *AQP1* in human retina specimens and cultured HRMECs**

310 To examine whether the AQP1 expression is correlated with diabetes in patients, we
311 measured its expression in diabetic and non-diabetic retina samples. In this study, a
312 total of 103 donors (n=54 in diabetic group and n=49 in non-diabetic group) were
313 enrolled. Fig.8A showed the representative fundus images and fluorescein angiograms
314 of non-diabetic retinas and diabetic subjects with different grades of DR, starting from
315 mild non-proliferative diabetic retinopathy (NPDR) to severe proliferative diabetic
316 retinopathy (PDR). The mean diameters of central retinal vessels (central retinal artery
317 and vein) and the retinal vessel branches (retinal arterioles and venules) were
318 measured (Fig.8B). There was no difference in the central retinal vessel between
319 diabetic and non-diabetic retina samples, whereas the diameter of the retinal vessel
320 branches was significantly decreased in diabetic retinas (Fig.8C and D). Next, the
321 mRNAs of both groups were isolated and applied to quantitative-PCR. The statistical
322 results demonstrated that the relative expression of *AQP1* was significantly lower in
323 diabetic samples than in non-diabetic samples (Fig.8E). The percentages of donors with
324 downregulated *AQP1* were 77.8% (42/54) and 42.9% (21/49) in diabetic and non-
325 diabetic groups, respectively (Table 1). The *AQP1* expression was negatively correlated
326 with diabetes (P=0.0003). Moreover, there was no difference between the groups in
327 terms of age and sex (P=0.3983 and P=0.3439, respectively) (Table 2). In the diabetic
328 group, 19 patients were diagnosed with NPDR and 35 patients were diagnosed with

329 PDR. However, there was no *AQP1* expression difference between NPDR patients (16
330 samples showed down-regulated *AQP1* expression) and PDR patients (26 samples
331 showed down-regulated *AQP1* expression).

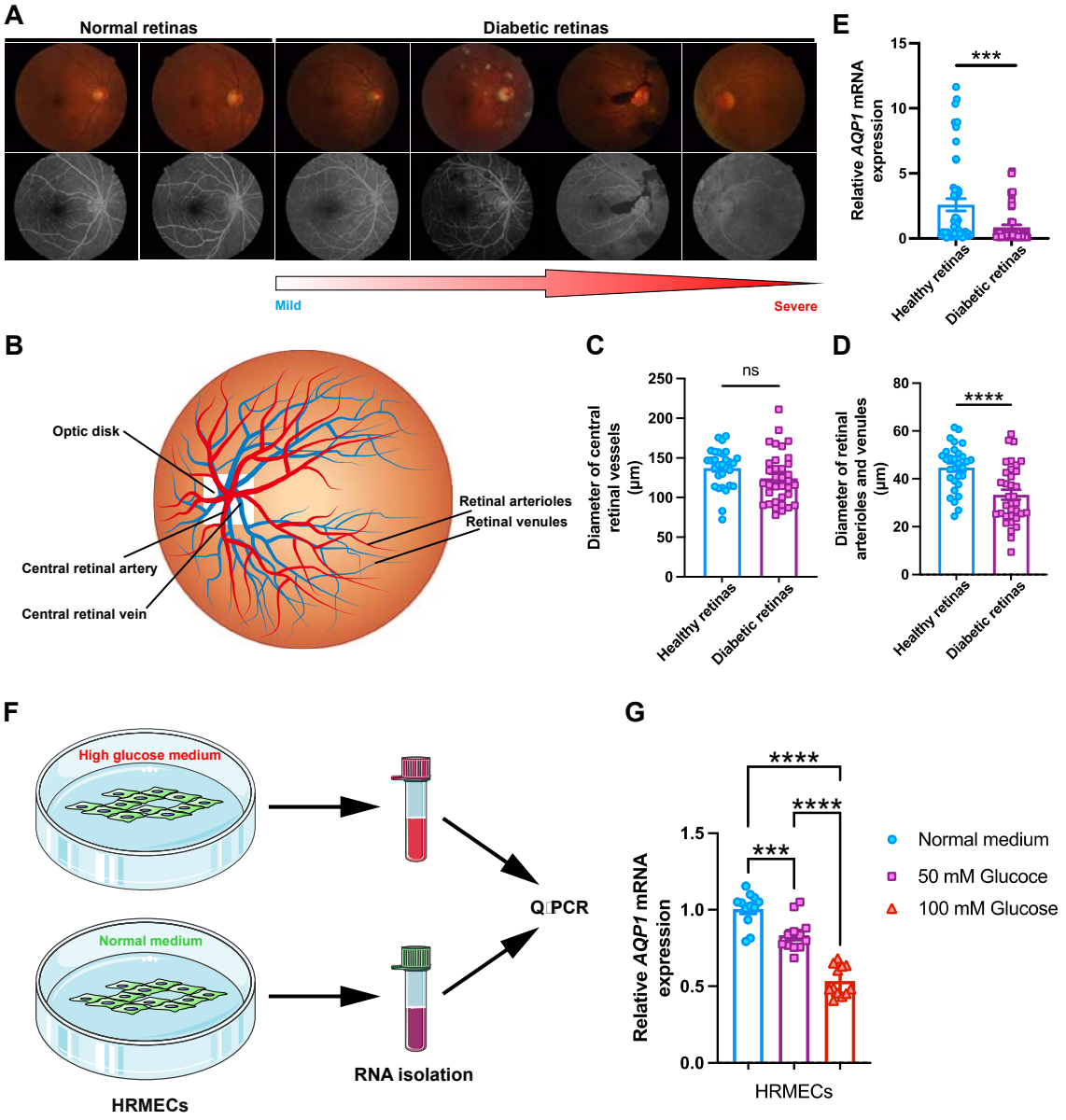

332

333 **Figure 8. *AQP1* expression is downregulated in retina samples from diabetic patients. A,**
334 Representative fundus images (upper) and fluorescein angiography (lower) of normal retinas
335 and retina with diabetic retinopathy (DR) at different stages (from mild to severe). **B,**
336 Representative sketch of human retinal vessels. **C,** Diameters of the central retinal vessels
337 (central retinal artery and vein) and the branching retinal vessels (retinal arterioles and venules).
338 Data are shown as mean ± s.e.m. A two-tailed, unpaired Student's t-test is applied. ns, not

339 significant. ****, p < 0.0001. **D,** Quantification of *AQP1* expression in healthy (n=49) and
340 diabetic (n=54) retina samples. Data are shown as mean ± s.e.m. A two-tailed, unpaired
341 Student's t-test is applied. ***, p < 0.001. **E,** Quantification of *AQP1* expression in HRMECs
342 cultured in normal and high glucose medium. One-way ANOVA analysis is applied. ****, p <
343 0.0001.

344

345 The expression of *AQP1* in endothelial cells under high glucose condition was further
346 assessed in cultured human retinal microvascular endothelial cells (HRMECs)
347 (Fig.8F). Compared with cells cultured in complete classic medium, high glucose-
348 treated cells displayed a lower *AQP1* expression (Fig.8G), consisting with our previous
349 results.

350 **Table 1 Differential expression of *AQP1* mRNA in non-diabetic and diabetic retinas**

Type	number	Relative expression		Negative	P
		<0.5[a]	>0.5		
Retinas from non-diabetic donors (Healthy subjects)	49	21	28	42.9%	0.0003
Retinas from diabetic donors (Diabetic subjects)	54	42	12	77.8%	χ^2=13.190

351 [a]Two-folds downregulated.
352

353 **Table 2 Correlation of *AQP1* expression with age and sex**

Group		number	Relative expression		Negative	P
			<0.5[a]	>0.5		
Age	≤64[b]	50	28	22	56.0%	0.3983
	>64	53	34	19	64.1%	χ^2=0.7143
Sex	Male	70	45	25	64.3%	0.3439
	Female	33	18	15	54.5%	χ^2=0.8958

354 [a]Two-folds downregulated; [b]Mean age.

355

356 ## Discussion

357 Diabetic retinopathy (DR) is a common vascular complication of diabetes and also a
358 leading cause of vision loss among working-age populations (Forbes and Cooper, 2013).

359 It is often accompanied by a series of retinal vascular lesions, including reduced vessel
360 perfusion, damaged vasculature, increased vascular permeability, and
361 neovascularization (Duh et al., 2017). Hyperglycemia is an inextricable reason for DR,
362 and the diameter changes in retinal vessels has been recognized as a clinical sign of
363 DR (Klein et al., 2012; Wong, 2011). In our study, we observed a significant
364 downregulation of *AQP1* in retinas from patients with diabetes and high glucose treated
365 HRMECs. These observations indicate a novel pathophysiological link between AQP1
366 and DR. Aquaporins (AQPs) belongs to a superfamily of major intrinsic proteins (MIPs)
367 and serves as channel proteins to transport water and/or small solutes across plasma
368 membrane (Papadopoulos et al., 2008; Reizer et al., 1993; Verkman, 2005). Based on
369 their abilities of transporting water or other solutes, such as glycerol, the aquaporin
370 superfamily can be divided into two subfamilies: aquaporins and aquaglyceroprins.
371 However, whether AQPs play roles in vascular luminization and pathological vascular
372 complications progression are poorly understood. Discoveries in vascular research have
373 been limited by a shortage of a model for imaging the blood vessels at high resolution *in*
374 *vivo*. To address this, the zebrafish model was utilized in our study, which offers
375 superior properties in cardiovascular research. In zebrafish, 14 of mammalian AQP
376 homologues have been cloned and their expression have been examined with WISH
377 (Qin et al., 2019). The unique spatio-temporal distribution of individual aquaporins
378 during zebrafish embryogenesis implied their distinct roles in the embryonic
379 development. Although aquaporins, particularly AQP1, have been reported to be
380 strongly expressed in ECs and proliferating tumor microvessels in humans (Nico and
381 Ribatti, 2010; Ribatti et al., 2014; Verkman, 2002; Verkman et al., 2008), their functions
382 in vascular system remain to be elucidated. Among all these aquaporin homologues,
383 zebrafish *aqp1a.1* and *aqp8a.1* were endothelium-enriched. To further investigate the
384 effects of EC-expressed Aqp1a.1 and Aqp8a.1 on angiogenesis during zebrafish
385 development, we examined the vascular phenotypic changes upon *aqp1a.1*/*aqp8a.1*
386 loss-of-function and gain-of-function. Either *aqp1a.1* or *aqp8a.1* disruption in zebrafish
387 embryos narrowed dorsal aorta, cardinal vein and ISVs, which were more sensitive to
388 AQPs loss of function. In contrast, overexpressing *aqp1a.1* or *aqp8a.1* leaded to
389 increases in vascular diameters. Moreover, blockage the function of AQPs by mercury

390 resulted in the luminization defect of blood vessel as well. Taken together, these
391 observations suggested that AQPs modulated the blood vessel lumenization during
392 both vasculogenesis and angiogenesis. In addition, both aqp1a.1 and apq8a.1 were
393 localized in the intracellular vacuoles in cultured ECs as well as the ECs of sprouting
394 ISVs, and loss of Aqps caused the reduction of those vacuoles. Since zebrafish ISVs
395 adopted the intracellular vacuoles fusion as the main strategy for vascular lumenization,
396 the -enriched Aqps might play a critical role in this biological process, supporting two
397 previous notions that the vascular lumen formation was driven by intercellular fusion of
398 endothelial vacuoles (Kamei et al., 2006) and AQP was expressed on cytoplasmic
399 vesicles and required for lumen extension (Khan et al., 2013).

400

401 Zebrafish has been widely used in diabetic studies (Jung et al., 2016; Lee and Yang,
402 2021; Wiggenhauser et al., 2020), and a hyperglycemic state and a series of diabetic
403 vascular complications can be easily simulated through immersing the zebrafish
404 embryos or adults in high concentrated glucose solution (Gleeson et al., 2007; Liang et
405 al., 2010). In our data, high glucose treatment led to the vascular defects which were
406 well matched with the luminization phenotype in *aqp1a.1*/*aqp8a.1* loss-of-function.
407 Under hyperglycemic condition, the IOC in eyes and ISVs were narrowed significantly.
408 Furthermore, we discovered that zebrafish *aqp1a.1* and *aqp8a.1* were downregulated
409 upon high glucose exposure, which was consistent with our observation that *AQP1* was
410 downregulated in human diabetic retinas and high glucose treated HRMECs. Most
411 importantly, overexpressing *aqp1a.1*, orthologous to human *AQP1*, in ECs of zebrafish
412 DM model could rescue the vascular defects. All these results were in support of the
413 viewpoint that EC-expressed aquaporins are correlated with hyperglycemia-related
414 vascular complications. Sada et al. have ever mentioned that overexpression of
415 AQP1 attenuates the hyperglycemia-induced vascular complications (Sada et al., 2016,
416 p. 1). In their proposed working model, hyperglycemia leads to high oxygen
417 consumption which promotes mitochondrial ROS production and induces cellular
418 hypoxia. Afterwards, the mitochondrial ROS and cellular hypoxia promote
419 the overproduction of endothelin-1 and fibronectin, and induce the apoptosis, which

420 further leads to diabetic vascular complications. Based on our data, the attenuated
421 hypoxia might due to improvement of the vascular perfusion induced by the
422 overexpression of AQP1. However, overexpression of AQP1 is able to suppress the
423 hypoxic state through functioning as the oxygen channel in ECs (Echevarría et al.,
424 2007), and then prevent the aforementioned hyperglycemia-induced vascular damages.
425 In addition to AQP1, other non-EC-expressed aquaporins are also associated with
426 diabetes. Zhang et al. have found that AQP11 was down-regulated in DR and resulted
427 in intracellular edema in DR subsequently (Zhang et al., 2022). AQP2 was also reported
428 to be involved in diabetic kidney diseases (Hadidi et al., 2022; Hinrichs et al., 2022).
429 However, to our knowledge, it was the first time that AQP1 was reported to be involved
430 in physiological as well as pathological vascular lumen formation.

431 Our investigations on retina samples from diabetic patients and zebrafish DM model
432 emphasized that the EC-enriched aquaporins are associated with vascular lumenization
433 defect in hyperglycemia. Functional inhibition of aquaporins recapitulated vascular
434 alterations of high-glucose treated zebrafish model, and overexpression of aquaporin in
435 ECs rescued the defect. In summary, current study suggests that EC-enriched
436 aquaporins have a role in developmental and pathological blood vessel lumenization,
437 and they might be potential targets for gene therapy to cure diabetes-related vascular
438 lumenization defects.

439

440 **Materials and Methods**

441 **Study approval**

442 Experiments involving human samples were approved by Affiliated Hospital of Nantong
443 University (2020-K013). Retina samples from 103 donors were obtained from Nanjing
444 Red Cross Eye Bank (Nanjing, China) between 2019 and 2021, and informed written
445 consent was obtained from each individual. The 49 non-diabetic retina donors included
446 31 males and 18 females (average age, 62; age range, 23-85 years), and the 54
447 diabetic donors included 39 males and 15 females (average age, 66; age range, 37-88
448 years). All animal experimentation was carried out in accordance with NIH Guidelines
449 for care and use of laboratory animals (http://oacu.od.nih.gov/regs/index.htm) and

450 ethically approved by the Administration Committee of Experimental Animals, Jiangsu
451 Province, China (Approval ID: SYXK(SU) 2017–111). Best efforts were made to
452 minimize the number of animals used and prevent their suffering.

453

454 **Zebrafish husbandry and strains**

455 The wild-type AB line and transgenic lines *Tg(kdrl:EGFP)* (Wang et al., 2016),
456 *Tg(fli1ep:EGFP-CAAX)*^{ntu666}, *Tg(fli1ep:aqp1a.1-mCherry)*^{ntu667}, *Tg(fli1ep:aqp8a.1-*
457 *EGFP)*^{ntu668}, and *Tg(fli1:EGFP–cdc42wt)* (Kamei et al., 2006) were used in this study.
458 All zebrafish embryos and adult fishes were raised and maintained at 28.5 ºC.

459

460 **Construction of transgenic lines**

461 *Tg(fli1ep:EGFP-CAAX)*^{ntu666} transgenic line was generated by injecting *pTol2-fli1ep-*
462 *EGFP-CAAX* into the progeny of wild-type AB line together with Tol2 transposase
463 mRNA into 1-cell stage wildtype fertilized eggs (1 ng / embryo) according to the Tol2kit
464 protocol (Kwan et al., 2007). *Tg(fli1ep:aqp1a.1-mCherry)* ^{ntu667} and *Tg(fli1ep:aqp8a.1-*
465 *mCherry)* ^{ntu668} transgenic lines were generated by using the same strategy (Fig.S6).

466

467 **High glucose treatment**

468 The zebrafish embryos were incubated at high glucose solution for 24 hours from 48 hpf
469 and imaged at 72 hpf. The embryos incubated in E3 medium were used as control. To
470 measure the glucose level in zebrafish embryos after glucose treatment, the embryos
471 were first sacrificed with rapid chilling (submerge fish embryos into 2-4 ºC chilled water).
472 Following confirmation of the absence of heart beat under a using a stereo microscope,
473 the embryos were rinsed with E3 medium twice and then dried with paper towel and
474 placed into 2-ml microcentrifuge tube. One-hundred embryos were collected for each
475 time point (48, 60, 72, 84, and 96 hpf, respectively) and divided into 5 groups (5
476 biological replicates). The embryos were homogenized and centrifuged to collect the
477 supernatant. Two microliter of the supernatant was placed on a glucometer strip (One-

478 Touch Ultra 2) and the glucose level was measured with a glucometer (One-Touch Ultra
479 2).

480

481 **ECs sorting, RNA extraction, RNA-seq, and qPCR**

482 To isolate ECs, the control and high-glucose treated *Tg(kdrl:EGFP)* embryos (300-400
483 embryos for each) were collected at 96 hpf, and followed by washing with PBC for three
484 times and digested with 0.25% trypsin at 37˚C. The digested cells were collected by
485 centrifugation and allowed to pass through a 40 mm FACS tube (BD Falcon, 352340).
486 The EGFP positive cells were sorted by fluorescence-activated cell sorting on FACS
487 Aria3 (BD Biosciences). Total mRNAs of the retina samples, zebrafish embryos (30
488 embryos a pool), or ECs were extracted with TRIzol Reagent (Invitrogen, USA) and
489 quantified and qualified by NanoDrop (ThermoFisher Scientific, USA) and 1% agarose
490 gel. To study gene expression changes after high glucose treatment, RNA-seq was
491 performed with the prepared mRNAs from 72 and 96 hpf-control and high glucose-
492 treated zebrafish embryos. Three independent replicates of the samples were analyzed
493 for each treatment. All RNA samples were submitted to GENEWIZ Science (Suzhou,
494 China), and deep sequencings were performed on an Illumina Hiseq2500. Quantitative
495 RT-PCR was performed using the corresponding primers listed in Supplementary Table
496 S1.

497

498 **Whole-mount in situ hybridization (WISH)**

499 WISH with antisense RNA probes was performed as described previously (Krueger et
500 al., 2011). Templates for making probe to detect the expression of aqp1a.1
501 (NM_207059.1) and aqp8a.1 (NM_001004661.1), was cloned from cDNA fragments.
502 Primers for WISH were listed in Supplementary Table S1. After hybridization, images of
503 the embryos were acquired with an Olympus stereomicroscope MVX10 equipped with
504 an Olympus DP71 camera.

505

506 **Generation of *aqp1a.1* or *aqp8a.1* knockout mutants**

507 To generate *aqp1a.1* or *aqp8a.1* gene mutant zebrafish, we used a CRISPR/Cas9-
508 mediated approach. CRISPR/Cas9 target sites designed to identify the sequences in
509 the second exon of *aqp1a.1* or *aqp8a.1*. Primers for single-RNA (sgRNA) synthesis
510 were listed in Supplementary Table S1. Each sgDNA were individually subcloned into
511 pT7 vector and transcribed into sgRNA in vitro using the T7 mMessage mMachine kit
512 (Ambion). Microinjection was performed with 1-cell stage zebrafish embryos and each
513 embryo was co-injected with 100 pg sgRNA and 200 pg Cas9 mRNA. G0 generations
514 were examined by PCR and subsequently Sanger sequencing. A mutant with 7 bp
515 deletion at the second exon of *aqp1a.1* which leads to the occurrence of a stop codon at
516 downstream of the Cas9 cutting site was identified. The heterozygous *aqp1a.1*$^{+/-}$
517 mutants were incrossed to obtain the homozygous F2 progenies.

518

519 **Morpholino-mediated gene knockdown of *aqp1a.1* or *aqp8a.1* in zebrafish**

520 The gene-specific morpholinos (Gene Tools, LLC) were used to block the splicing of the
521 pre-mRNA. Morpholino antisense oligomers (refer to as MO) were prepared according
522 to the manufacturer's instruction. The MO sequences used were listed Supplementary
523 Table S1. In this experiment, 2 nL of 0.3 mM morpholino oligo was microinjected into
524 the embryos at the 1-cell stage.

525

526 **$HgCl_2$ treatment**

527 Functional inhibition of Aqp1a.1 and Aqp8a.1 using HgCl2 was performed with
528 dechorionated embryos at 22 hpf in E3 medium. Three different HgCl2 concentrations
529 (0.2, 0.4, and 1.6 μM) were used. The embryos were incubated in the HgCl2-containing
530 E3 medium from 22 hpf and imaged at 48 hpf.

531

532 **Microangiography and confocal imaging**

533 For confocal imaging of blood vessel development, zebrafish embryos treated with 1-
534 phenyl-2-thiourea (Sigma Aldrich) to inhibit the pigmentation. After manually
535 dechorionation, embryos were anesthetized with egg water/0.16 mg/ml tricaine/1% 1-
536 phenyl-2-thiourea (Sigma) and embedded in 0.6% low melting agarose. For
537 microangiography, 5 μg/μl Dextran TexasRed (Invitrogen) was injected into the common
538 cardinal vein (CCV) at 72 hpf and immediately processed for optical imaging. Living
539 imaging was performed with Nikon A1R confocal microscopy.

540

541 **Quantitative analysis of blood vessel diameter**

542 The vessel diameters were quantified in Fiji using the Vessel Analysis plugin (Schindelin
543 et al., 2012). For zebrafish, 5 locations on IOC, DA and PCV were selected and
544 measured. For zebrafish ISV diameter measurement, 5 ISVs beyond the yolk yac
545 extension were selected and an individual ISV was measured at 5 positions. A total of 5
546 fishes were applied in each group. The average of these data points was statistically
547 used as the diameter of the analyzed vessel. For human retinal vessels, measurements
548 were carried out on fluorescein angiograms. The mean diameters of the central retinal
549 vessels in the optic disk and the branching retinal vessels were separately calculated.
550 The vascular perfusion analysis in zebrafish was based on the microangiographic
551 images. Completely or partially lost the red fluorescence in ISV was defined as
552 defective-perfused ISV.

553

554 **Cell culture and transfection**

555 Human umbilical vein endothelial cells (HUVECs, Cell System) were cultured in in
556 endothelial cell growth medium according to the protocol provided by the manufacturer
557 (VascuLife, Cell System). Lipofectamine™ 3000 Transfection Reagent (ThermoFisher
558 Scientific) was used for plasmid transfection. The *aqp1a.1* or *aqp8a.1* cDNA was
559 subcloned into pmCherry-N1 or pEGFP-N1 vector (Addgene). Human retinal
560 microvascular endothelial cells (HRMECs, Cell System) were cultured in complete
561 classic medium supplemented with/without high content glucose (50 or 100 mM). Cells

562 were incubated in normal medium and high glucose medium for 48 h and subjected to
563 RNA extraction.

564

565 **Statistical analysis**

566 Statistical analysis employed a two-tailed, unpaired Student's t-test, One-way ANOVA,
567 or Fisher's exact test are described in figure legends. Chi square test ($\chi 2$-value) was
568 used for intergroup comparison of categorical data. All data are presented as mean ±
569 s.e.m. $P<0.05$ was considered to be statistically significant.

570

571 **Acknowledgements**

572 This study was supported by grants from the National Natural Science Foundation of
573 China (https://www.nsfc.gov.cn/; 81870359 and 2018YFA0801004 received by DL;
574 82000458 received by CC). The funders had no role in study design, data collection and
575 analysis, decision to publish, or preparation of the manuscript.

576

577 **Author Contributions**

578 DL supervised and designed this project. CC, DL , YQ wrote the manuscript. DL, CC,
579 and YX analyzed the data. CC, YQ and YX performed the experiments; YX, LC and LW
580 collected the clinical data.

581

582 **Conflicts of Interest**

583 The Authors declare that there is no conflict of interest.

584

585 **References**

586 Agemy SA, Scripsema NK, Shah CM, Chui T, Garcia PM, Lee JG, Gentile RC, Hsiao Y-
587 S, Zhou Q, Ko T, Rosen RB. 2015. Retinal vascular perfusion density mapping

588 using optical coherence tomography angiography in normals and diabetic
589 retinopathy patients. *Retina* **35**:2353–2363. doi:10.1097/IAE.0000000000000862
590 Beckman JA, Creager MA. 2016. Vascular Complications of Diabetes. *Circ Res*
591 **118**:1771–1785. doi:10.1161/CIRCRESAHA.115.306884
592 Chen C, Liu D. 2022. Establishment of Zebrafish Models for Diabetes Mellitus and Its
593 Microvascular Complications. *J Vasc Res* **59**:1–9. doi:10.1159/000522471
594 Duh EJ, Sun JK, Stitt AW. 2017. Diabetic retinopathy: current understanding,
595 mechanisms, and treatment strategies. *JCI Insight* **2**:e93751.
596 doi:10.1172/jci.insight.93751
597 Echevarría M, Muñoz-Cabello AM, Sánchez-Silva R, Toledo-Aral JJ, López-Barneo J.
598 2007. Development of cytosolic hypoxia and hypoxia-inducible factor stabilization
599 are facilitated by aquaporin-1 expression. *J Biol Chem* **282**:30207–30215.
600 doi:10.1074/jbc.M702639200
601 Forbes JM, Cooper ME. 2013. Mechanisms of Diabetic Complications. *Physiological*
602 *Reviews* **93**:137–188. doi:10.1152/physrev.00045.2011
603 Gleeson M, Connaughton V, Arneson LS. 2007. Induction of hyperglycaemia in
604 zebrafish (Danio rerio) leads to morphological changes in the retina. *Acta*
605 *Diabetol* **44**:157–163. doi:10.1007/s00592-007-0257-3
606 Gore AV, Monzo K, Cha YR, Pan W, Weinstein BM. 2012. Vascular development in the
607 zebrafish. *Cold Spring Harbor Perspectives in Medicine* **2**:1–21.
608 doi:10.1101/cshperspect.a006684
609 Hadidi H, Kamali R, Binesh A. 2022. Dynamics and energetics of water transport
610 through aquaporin mutants causing nephrogenic diabetes insipidus (NDI): A
611 molecular dynamics study. *J Biomol Struct Dyn* **40**:1273–1284.
612 doi:10.1080/07391102.2020.1824813
613 Hinrichs GR, Baltzer S, Pallien T, Svenningsen P, Dalgaard EB, Hertz JM, Bistrup C,
614 Jensen BL, Klussmann E. 2022. A Novel AQP2 Sequence Variant Causing
615 Aquaporin-2 Retention in the Cytoplasm and Autosomal Dominant Nephrogenic
616 Diabetes Insipidus. *Kidney Int Rep* **7**:2289–2294. doi:10.1016/j.ekir.2022.07.001
617 Jung S-H, Kim YS, Lee Y-R, Kim JS. 2016. High glucose-induced changes in hyaloid-
618 retinal vessels during early ocular development of zebrafish: a short-term animal

619 model of diabetic retinopathy: HG-induced changes in hyaloid-retinal vessels in
620 ZF. *British Journal of Pharmacology* **173**:15–26. doi:10.1111/bph.13279
621 Kamei M, Brian Saunders W, Bayless KJ, Dye L, Davis GE, Weinstein BM. 2006.
622 Endothelial tubes assemble from intracellular vacuoles in vivo. *Nature* **442**:453–
623 456. doi:10.1038/nature04923
624 Khan LA, Zhang H, Abraham N, Sun L, Fleming JT, Hall DH, Gobel V. 2013.
625 Intracellular lumen extension requires ERM-1-dependent apical membrane
626 expansion and AQP-8-mediated flux **15**:143–156.
627 Klein R, Myers CE, Lee KE, Gangnon R, Klein BEK. 2012. Changes in Retinal Vessel
628 Diameter and Incidence and Progression of Diabetic Retinopathy. *Arch*
629 *Ophthalmol* **130**. doi:10.1001/archophthalmol.2011.2560
630 Krueger J, Liu D, Scholz K, Zimmer A, Shi Y, Klein C, Siekmann A, Schulte-merker S,
631 Cudmore M, Ahmed A, Noble F. 2011. Flt1 acts as a negative regulator of tip cell
632 formation and branching morphogenesis in the zebrafish embryo **2120**:2111–
633 2120. doi:10.1242/dev.063933
634 Kwan KM, Fujimoto E, Grabher C, Mangum BD, Hardy ME, Campbell DS, Parant JM,
635 Yost HJ, Kanki JP, Chien C-B. 2007. The Tol2kit: a multisite gateway-based
636 construction kit for Tol2 transposon transgenesis constructs. *Dev Dyn* **236**:3088–
637 3099. doi:10.1002/dvdy.21343
638 Lee Y, Yang J. 2021. Development of a zebrafish screening model for diabetic
639 retinopathy induced by hyperglycemia: Reproducibility verification in animal
640 model. *Biomedicine & Pharmacotherapy* **135**:111201.
641 doi:10.1016/j.biopha.2020.111201
642 Liang J, Gui Y, Wang W, Gao S, Li J, Song H. 2010. Elevated glucose induces
643 congenital heart defects by altering the expression of tbx5, tbx20, and has2 in
644 developing zebrafish embryos. *Birth Defects Res A Clin Mol Teratol* **88**:480–486.
645 doi:10.1002/bdra.20654
646 Liu J, Stainier DYR. 2012. Zebrafish in the study of early cardiac development.
647 *Circulation Research* **110**:870–874. doi:10.1161/CIRCRESAHA.111.246504

648 Liu K, Nagase H, Huang CG, Calamita G, Agre P. 2006. Purification and functional
649 characterization of aquaporin-8. *Biology of the Cell* **98**:153–161.
650 doi:https://doi.org/10.1042/BC20050026
651 Nico B, Ribatti D. 2010. Aquaporins in tumor growth and angiogenesis. *Cancer Letters*
652 **294**:135–138. doi:10.1016/j.canlet.2010.02.005
653 Osmani N, Péglion F, Chavrier P, Etienne-Manneville S. 2010. Cdc42 localization and
654 cell polarity depend on membrane traffic. *The Journal of cell biology* **191**:1261–9.
655 doi:10.1083/jcb.201003091
656 Papadopoulos MC, Saadoun S, Verkman AS. 2008. Aquaporins and cell migration.
657 *Pflugers Arch - Eur J Physiol* **456**:693–700. doi:10.1007/s00424-007-0357-5
658 Preston GM, Carroll TP, Guggino WB, Agre P. 1992. Appearance of water channels in
659 Xenopus oocytes expressing red cell CHIP28 protein. *Science* **256**:385–387.
660 doi:10.1126/science.256.5055.385
661 Qin Y, Wang S, Duan X, Liu D. 2019. Expression analysis of the aquaporins during
662 zebrafish embryonic development. *Gene Expression Patterns* **32**:38–43.
663 doi:10.1016/j.gep.2019.04.001
664 Reizer J, Reizer A, Saier MH. 1993. The MIP family of integral membrane channel
665 proteins: sequence comparisons, evolutionary relationships, reconstructed
666 pathway of evolution, and proposed functional differentiation of the two repeated
667 halves of the proteins. *Crit Rev Biochem Mol Biol* **28**:235–257.
668 doi:10.3109/10409239309086796
669 Ribatti D, Ranieri G, Annese T, Nico B. 2014. Aquaporins in cancer. *Biochimica et*
670 *Biophysica Acta (BBA) - General Subjects* **1840**:1550–1553.
671 doi:10.1016/j.bbagen.2013.09.025
672 Sada K, Nishikawa T, Kukidome D, Yoshinaga T, Kajihara N, Sonoda K, Senokuchi T,
673 Motoshima H, Matsumura T, Araki E. 2016. Hyperglycemia Induces Cellular
674 Hypoxia through Production of Mitochondrial ROS Followed by Suppression of
675 Aquaporin-1. *PLoS One* **11**:e0158619. doi:10.1371/journal.pone.0158619
676 Schindelin J, Arganda-Carreras I, Frise E, Kaynig V, Longair M, Pietzsch T, Preibisch S,
677 Rueden C, Saalfeld S, Schmid B, Tinevez J-Y, White DJ, Hartenstein V, Eliceiri K,

678 Tomancak P, Cardona A. 2012. Fiji: an open-source platform for biological-image
679 analysis. *Nat Methods* **9**:676–682. doi:10.1038/nmeth.2019
680 Smith BL, Agre P. 1991. Erythrocyte Mr 28,000 transmembrane protein exists as a
681 multisubunit oligomer similar to channel proteins. *Journal of Biological Chemistry*
682 **266**:6407–6415. doi:10.1016/S0021-9258(18)38133-X
683 Toh H, Smolentsev A, Bozadjian RV, Keeley PW, Lockwood MD, Sadjadi R, Clegg DO,
684 Blodi BA, Coffey PJ, Reese BE, Thomson JA. 2019. Vascular changes in
685 diabetic retinopathy—a longitudinal study in the Nile rat. *Lab Invest* **99**:1547–
686 1560. doi:10.1038/s41374-019-0264-3
687 Verkman AS. 2005. More than just water channels: unexpected cellular roles of
688 aquaporins. *Journal of Cell Science* **118**:3225–3232. doi:10.1242/jcs.02519
689 Verkman AS. 2002. Aquaporin water channels and endothelial cell function*. *J Anatomy*
690 **200**:617–627. doi:10.1046/j.1469-7580.2002.00058.x
691 Verkman AS, Hara-Chikuma M, Papadopoulos MC. 2008. Aquaporins—new players in
692 cancer biology. *J Mol Med* **86**:523–529. doi:10.1007/s00109-008-0303-9
693 Wang W, Lo ACY. 2018. Diabetic Retinopathy: Pathophysiology and Treatments. *Int J*
694 *Mol Sci* **19**:1816. doi:10.3390/ijms19061816
695 Wang X, Ling CC, Li L, Qin Y, Qi J, Liu X, You B, Shi Y, Zhang J, Jiang Q, Xu H, Sun C,
696 You Y, Chai R, Liu D. 2016. MicroRNA-10a / 10b represses a novel target gene
697 mib1 to regulate angiogenesis **1**:140–150. doi:10.1093/cvr/cvw023
698 Wiggenhauser LM, Qi H, Stoll SJ, Metzger L, Bennewitz K, Poschet G, Krenning G,
699 Hillebrands J-L, Hammes H-P, Kroll J. 2020. Activation of Retinal Angiogenesis
700 in Hyperglycemic *pdx1* $^{-/-}$ Zebrafish Mutants. *Diabetes* **69**:1020–1031.
701 doi:10.2337/db19-0873
702 Wong TY. 2011. Retinal Vessel Diameter as a Clinical Predictor of Diabetic Retinopathy
703 Progression: Time to Take Out the Measuring Tape. *Arch Ophthalmol* **129**:95.
704 doi:10.1001/archophthalmol.2010.347
705 Yang B, Kim JK, Verkman AS. 2006. Comparative efficacy of $HgCl_2$ with candidate
706 aquaporin-1 inhibitors DMSO, gold, TEA^+ and acetazolamide. *FEBS Letters*
707 **580**:6679–6684. doi:10.1016/j.febslet.2006.11.025

708 Zhang C, Luo D, Xie H, Yang Q, Liu D, Tang L, Zhang Jingting, Li W, Tian H, Lu L, Sun
709 X, Xu G-T, Zhang Jingfa. 2022. Aquaporin 11 alleviates retinal Müller intracellular
710 edema through water efflux in diabetic retinopathy. *Pharmacol Res* **187**:106559.
711 doi:10.1016/j.phrs.2022.106559
712

713

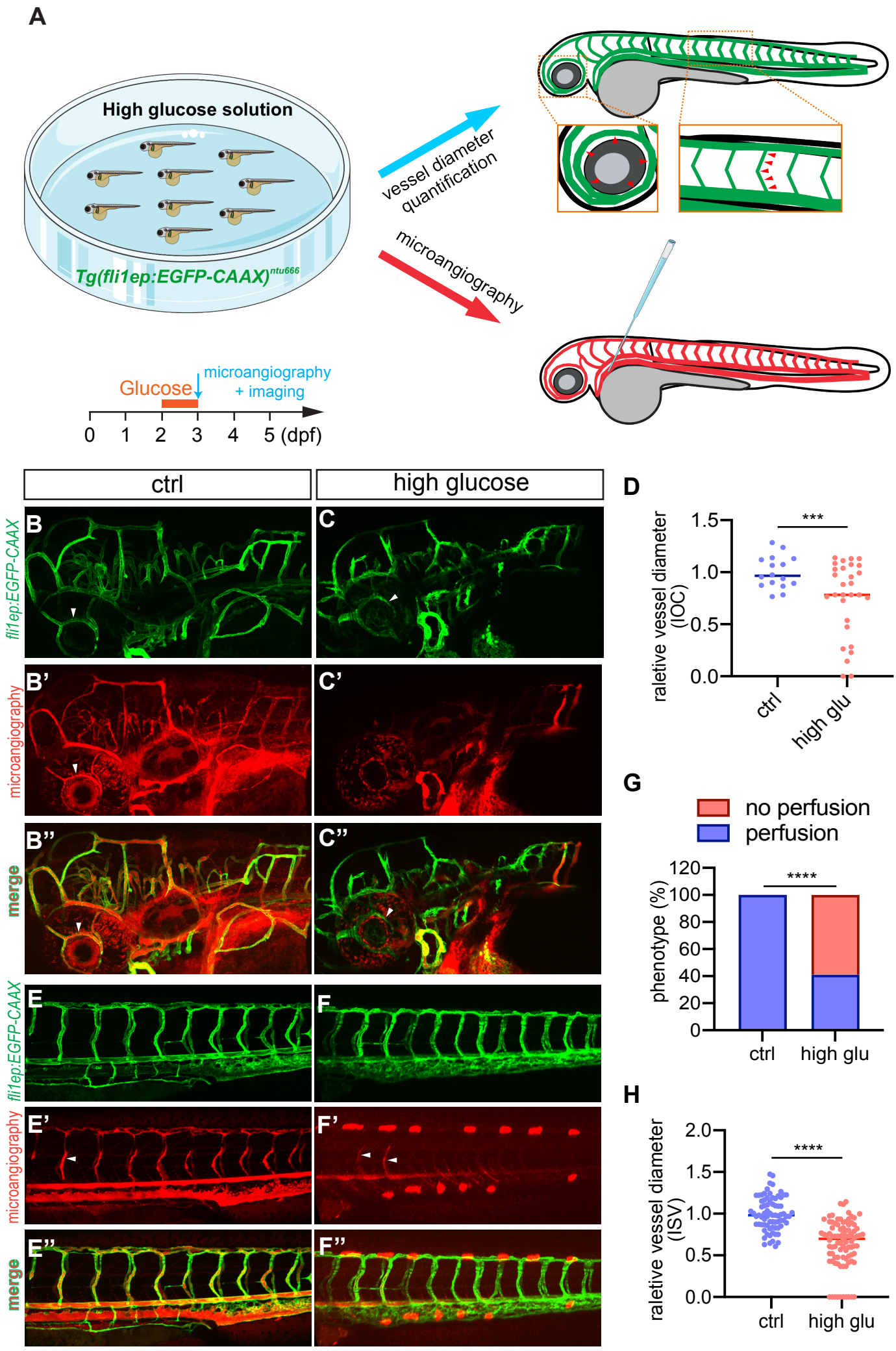
A
High glucose solution
Tg(fli1ep:EGFP-CAAX)ntu666
vessel diameter quantification
microangiography
Glucose
microangiography + imaging
0 1 2 3 4 5 (dpf)
ctrl
high glucose
fli1ep:EGFP-CAAX
microangiography
merge
B
C
B'
C'
B''
C''
E
F
E'
F'
E''
F''
D
raletive vessel diameter (IOC)
1.5
1.0
0.5
0.0
***
ctrl
high glu
G
no perfusion
perfusion
phenotype (%)
120
100
80
60
40
20
0
****
ctrl
high glu
H
raletive vessel diameter (ISV)
2.0
1.5
1.0
0.5
0.0
****
ctrl
high glu

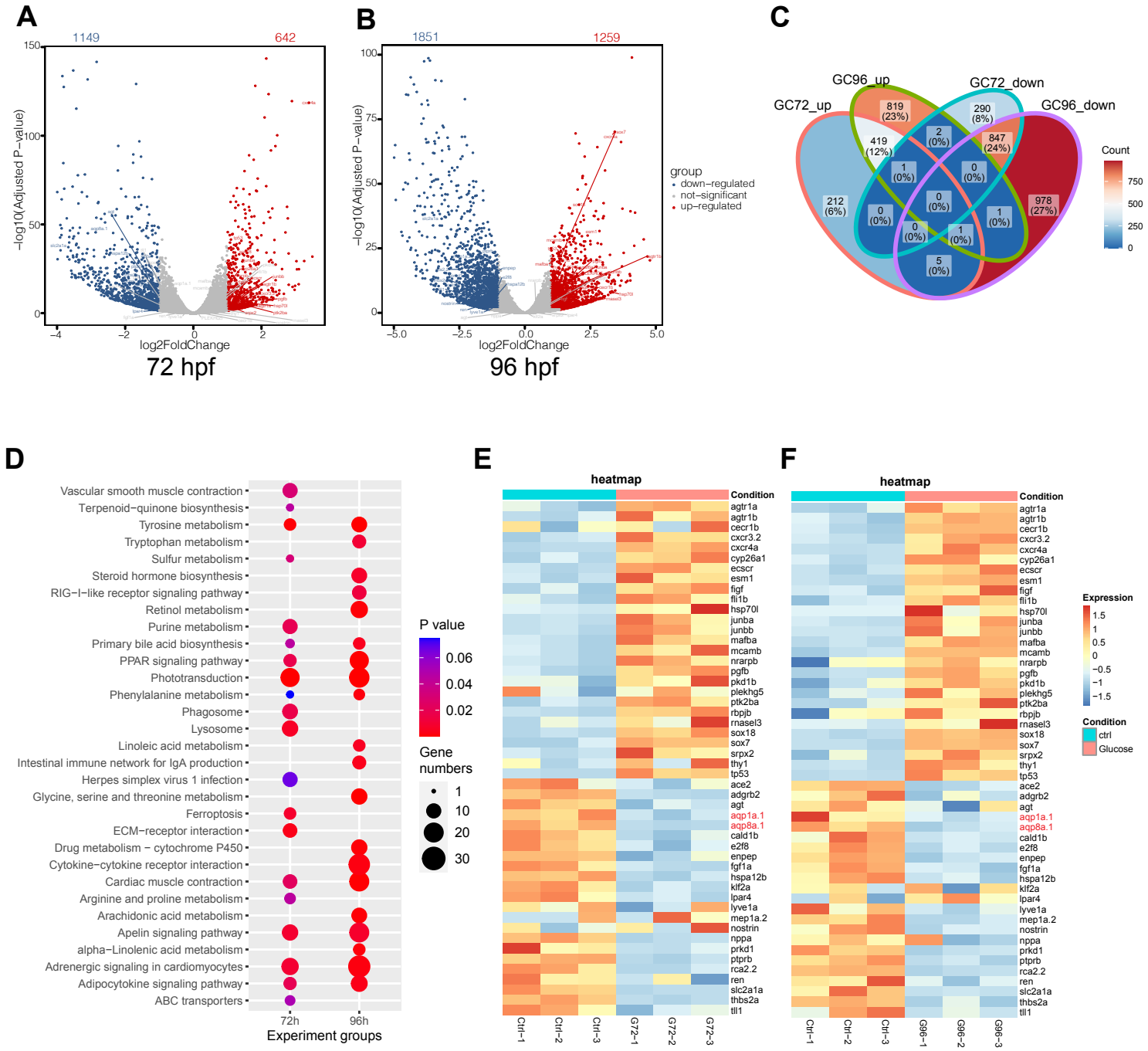
A
1149
642
−log10(Adjusted P−value)
log2FoldChange
72 hpf
B
1851
1259
−log10(Adjusted P−value)
log2FoldChange
96 hpf
group
down−regulated
not−significant
up−regulated
C
GC72_up
GC96_up
GC72_down
GC96_down
Count
D
Vascular smooth muscle contraction
Terpenoid−quinone biosynthesis
Tyrosine metabolism
Tryptophan metabolism
Sulfur metabolism
Steroid hormone biosynthesis
RIG−I−like receptor signaling pathway
Retinol metabolism
Purine metabolism
Primary bile acid biosynthesis
PPAR signaling pathway
Phototransduction
Phenylalanine metabolism
Phagosome
Lysosome
Linoleic acid metabolism
Intestinal immune network for IgA production
Herpes simplex virus 1 infection
Glycine, serine and threonine metabolism
Ferroptosis
ECM−receptor interaction
Drug metabolism − cytochrome P450
Cytokine−cytokine receptor interaction
Cardiac muscle contraction
Arginine and proline metabolism
Arachidonic acid metabolism
Apelin signaling pathway
alpha−Linolenic acid metabolism
Adrenergic signaling in cardiomyocytes
Adipocytokine signaling pathway
ABC transporters
72h
96h
Experiment groups
P value
Gene numbers
E
heatmap
Condition
F
heatmap
Condition
Expression
Condition
ctrl
Glucose

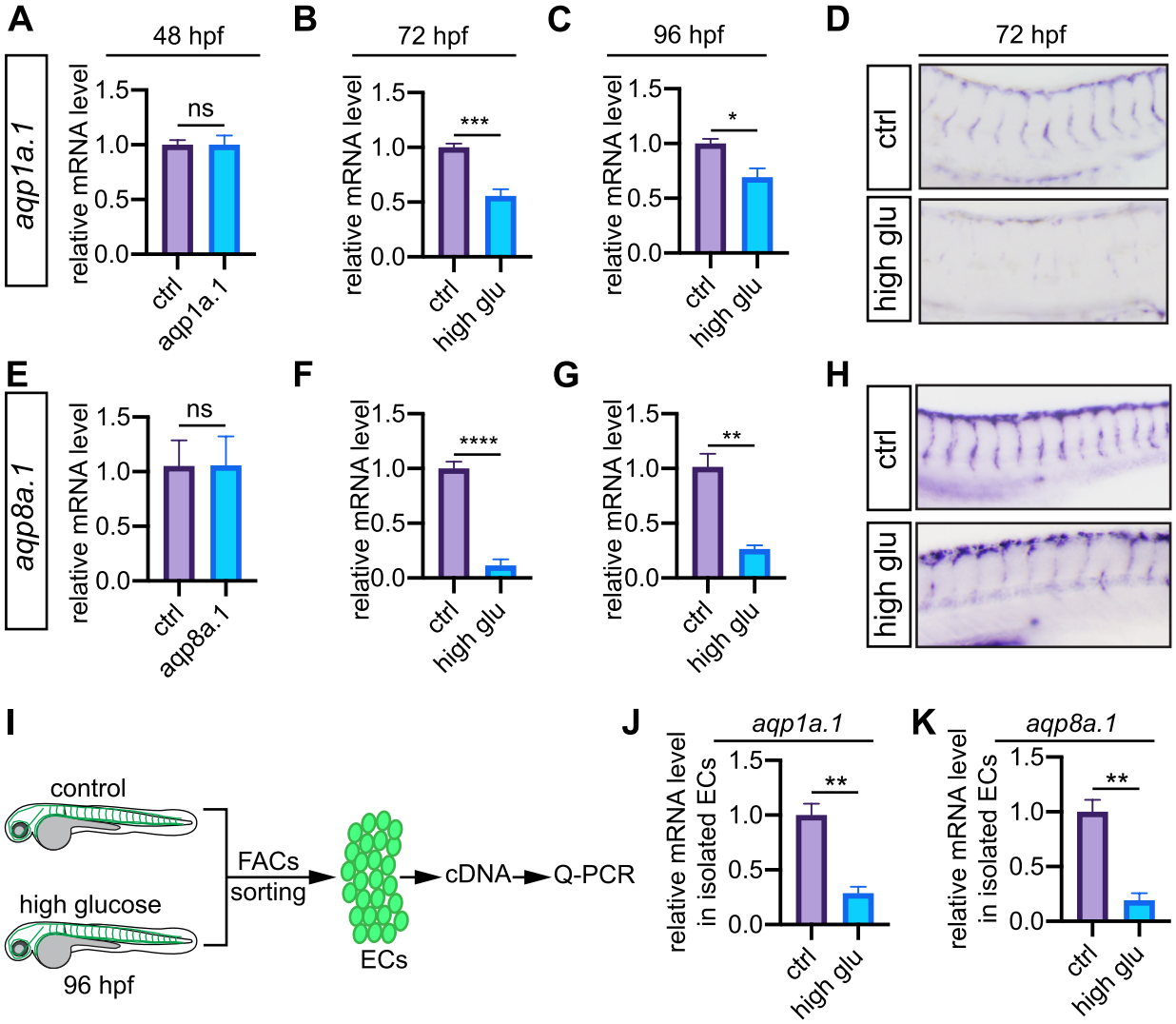
A
48 hpf
aqp1a.1
relative mRNA level
1.5
1.0
0.5
0.0
ns
ctrl
aqp1a.1
B
72 hpf
***
ctrl
high glu
C
96 hpf
*
D
72 hpf
ctrl
high glu
E
aqp8a.1
ns
F
****
G
**
H
I
control
high glucose
96 hpf
FACs
sorting
ECs
cDNA
Q-PCR
J
aqp1a.1
relative mRNA level
in isolated ECs
K
aqp8a.1

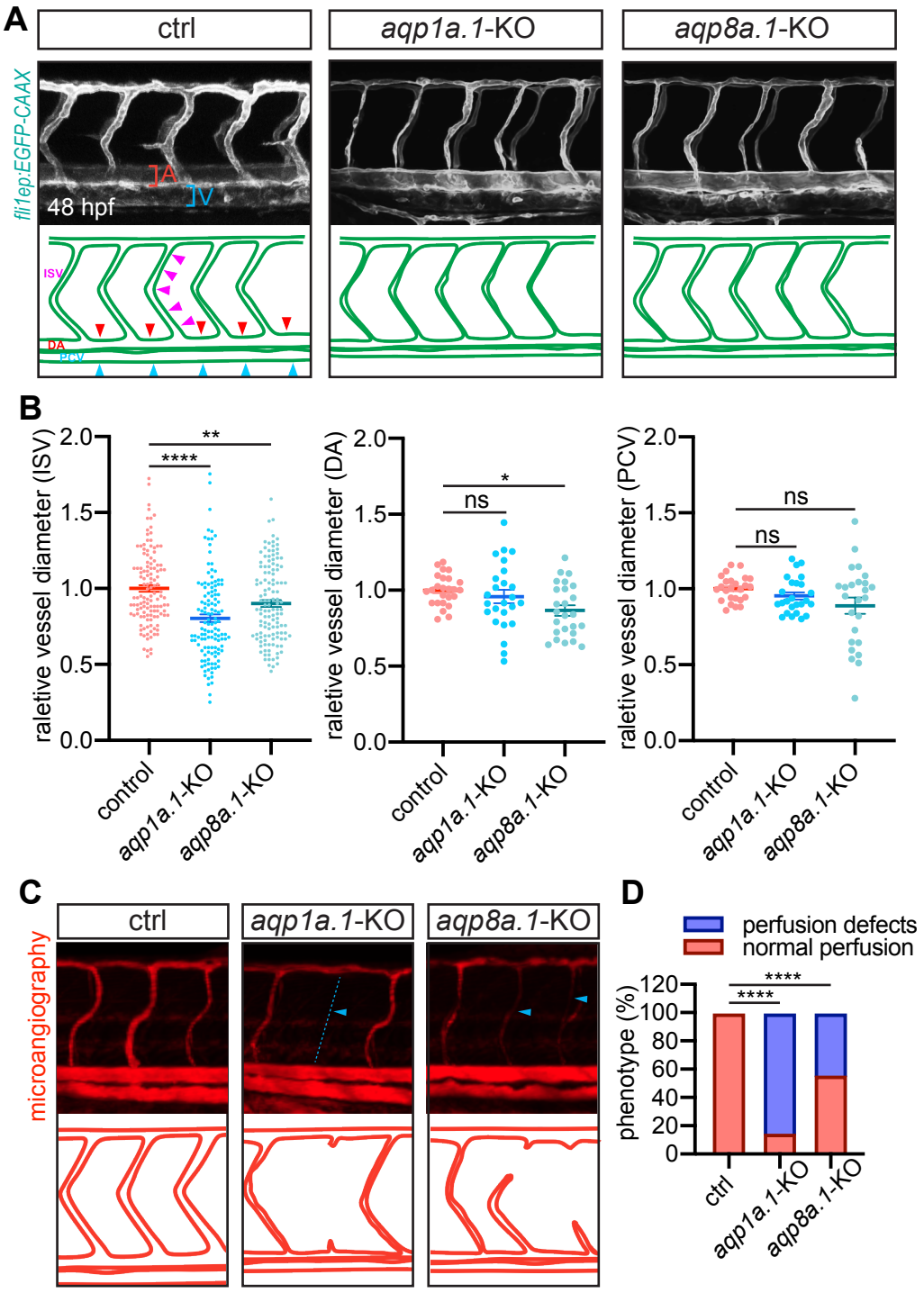
A
ctrl
aqp1a.1-KO
aqp8a.1-KO
fli1ep:EGFP-CAAX
48 hpf
DA
DV
ISV
DA
PCV
B
raletive vessel diameter (ISV)
raletive vessel diameter (DA)
raletive vessel diameter (PCV)
2.0
1.5
1.0
0.5
0.0
**
****
*
ns
ns
ns
control
aqp1a.1-KO
aqp8a.1-KO
C
ctrl
aqp1a.1-KO
aqp8a.1-KO
microangiography
D
perfusion defects
normal perfusion
phenotype (%)
120
100
80
60
40
20
0
****
****
ctrl
aqp1a.1-KO
aqp8a.1-KO

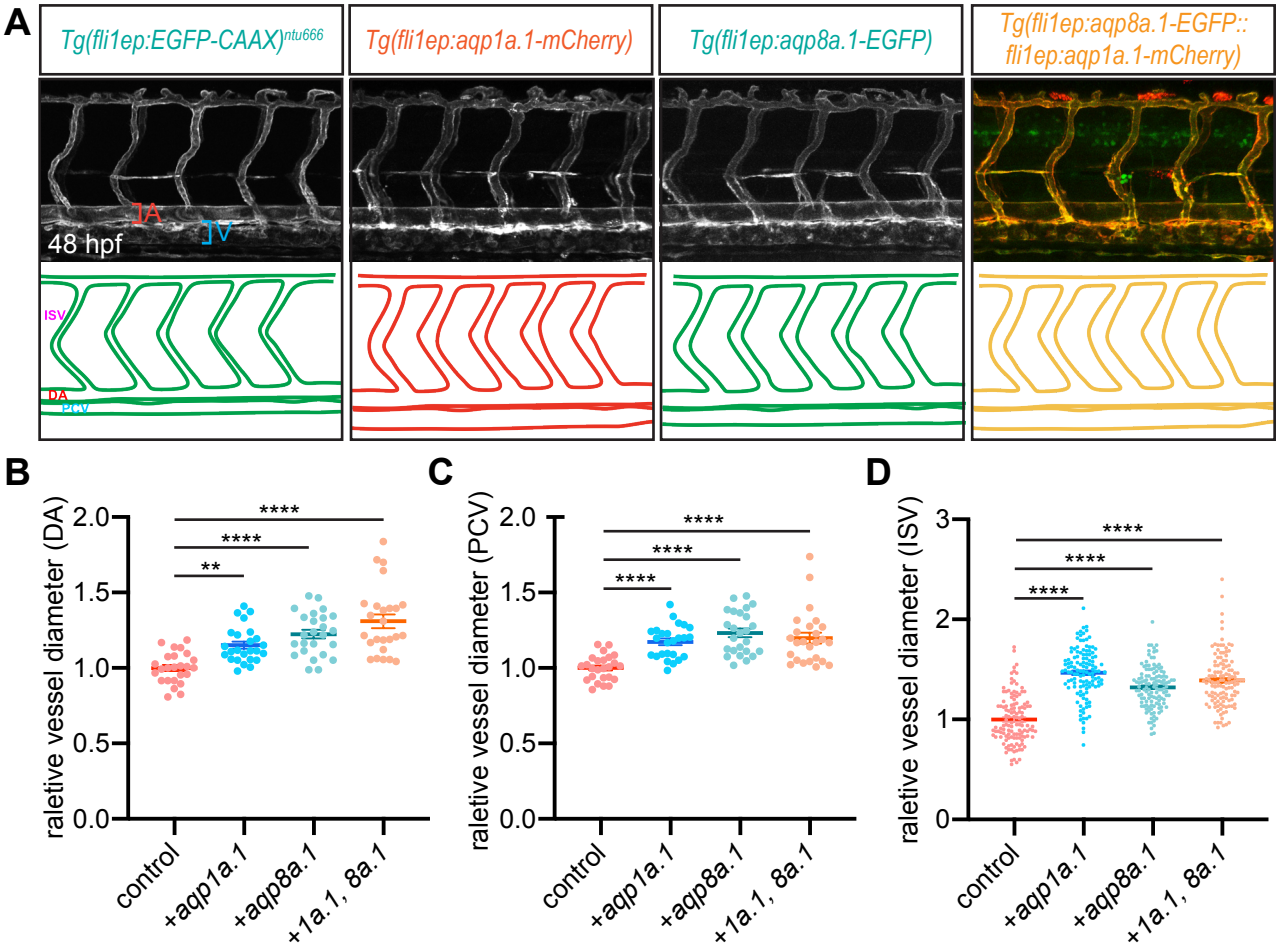
A
Tg(fli1ep:EGFP-CAAX)ntu666
Tg(fli1ep:aqp1a.1-mCherry)
Tg(fli1ep:aqp8a.1-EGFP)
Tg(fli1ep:aqp8a.1-EGFP::
fli1ep:aqp1a.1-mCherry)
48 hpf
DA
PCV
ISV
B
raletive vessel diameter (DA)
C
raletive vessel diameter (PCV)
D
raletive vessel diameter (ISV)
control
+aqp1a.1
+aqp8a.1
+1a.1, 8a.1
****
**

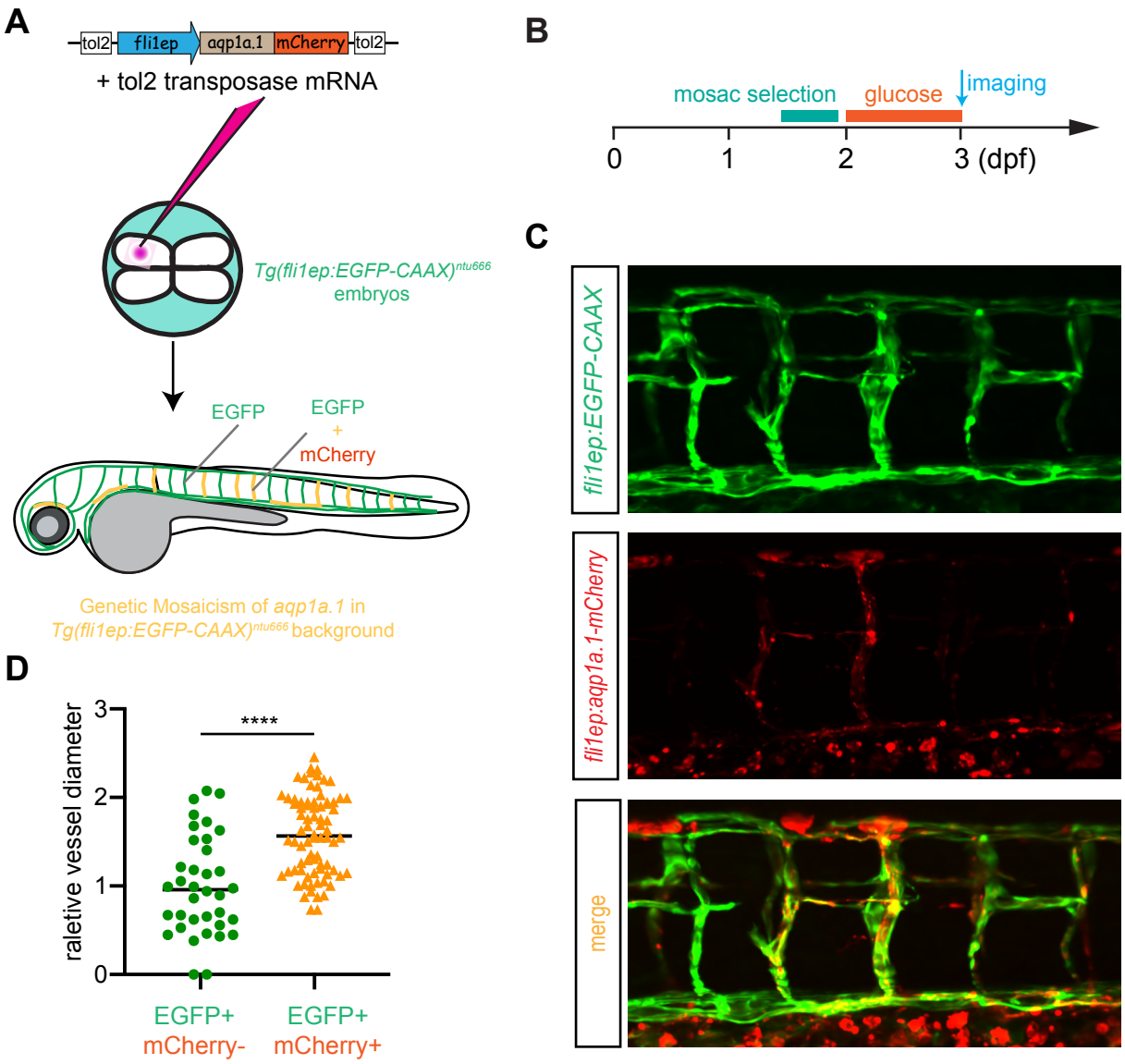
A
tol2
fli1ep
aqp1a.1
mCherry
tol2
+ tol2 transposase mRNA
Tg(fli1ep:EGFP-CAAX)ntu666
embryos
EGFP
EGFP
+
mCherry
Genetic Mosaicism of aqp1a.1 in
Tg(fli1ep:EGFP-CAAX)ntu666 background
B
mosac selection
glucose
imaging
0
1
2
3 (dpf)
C
fli1ep:EGFP-CAAX
fli1ep:aqp1a.1-mCherry
merge
D
raletive vessel diameter
3
2
1
0
****
EGFP+
mCherry-
EGFP+
mCherry+

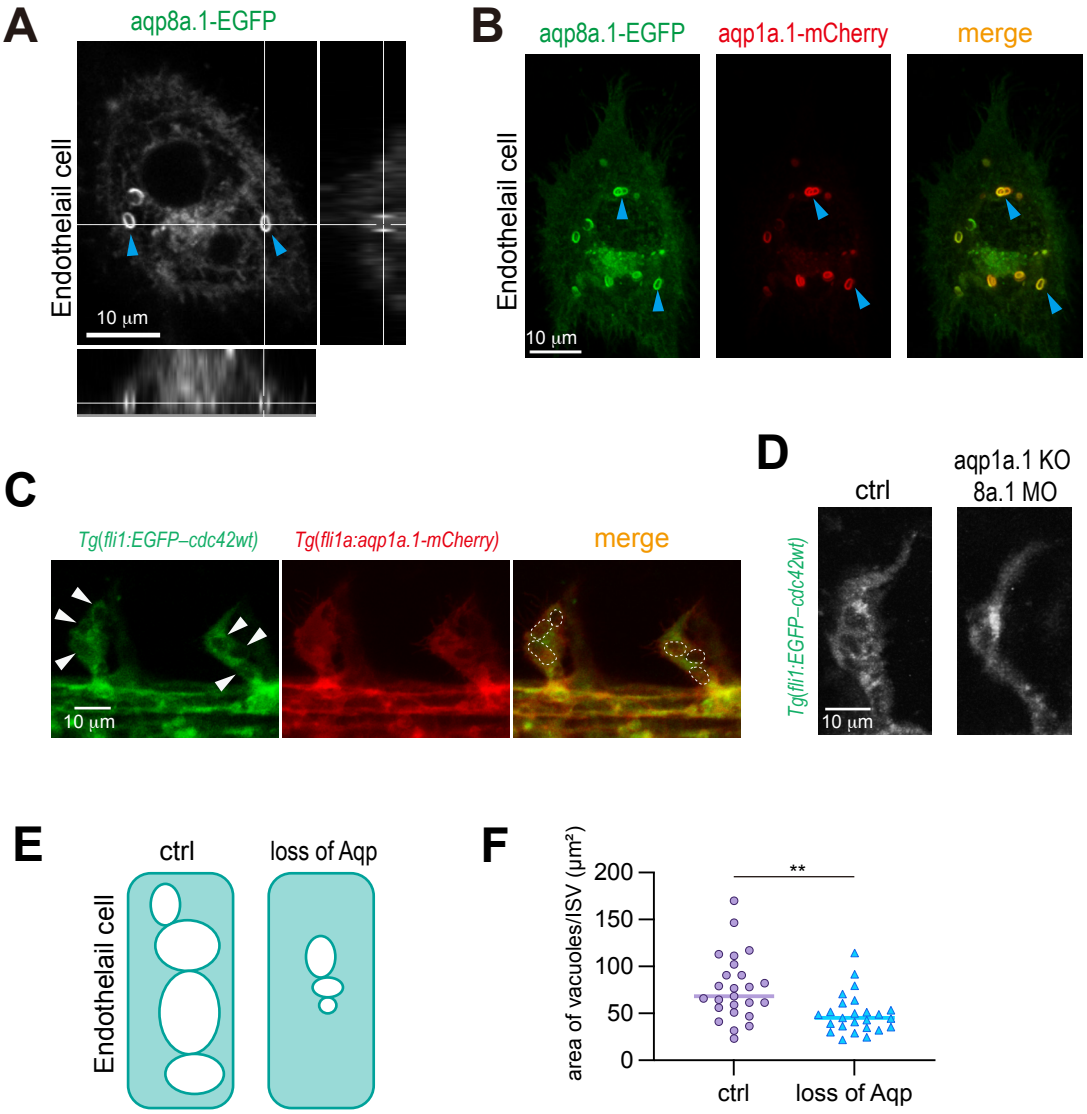
A
aqp8a.1-EGFP
Endothelail cell
10 μm
B
aqp8a.1-EGFP
aqp1a.1-mCherry
merge
Endothelail cell
10 μm
C
Tg(fli1:EGFP–cdc42wt)
Tg(fli1a:aqp1a.1-mCherry)
merge
10 μm
D
ctrl
aqp1a.1 KO
8a.1 MO
Tg(fli1:EGFP–cdc42wt)
10 μm
E
ctrl
loss of Aqp
Endothelail cell
F
area of vacuoles/ISV (μm²)
200
150
100
50
0
**
ctrl
loss of Aqp

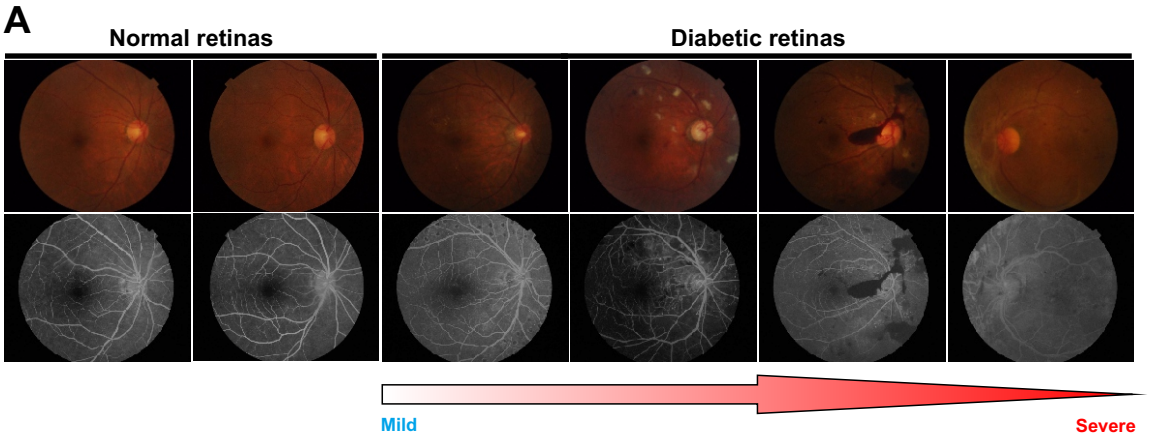
A
Normal retinas
Diabetic retinas
Mild
Severe

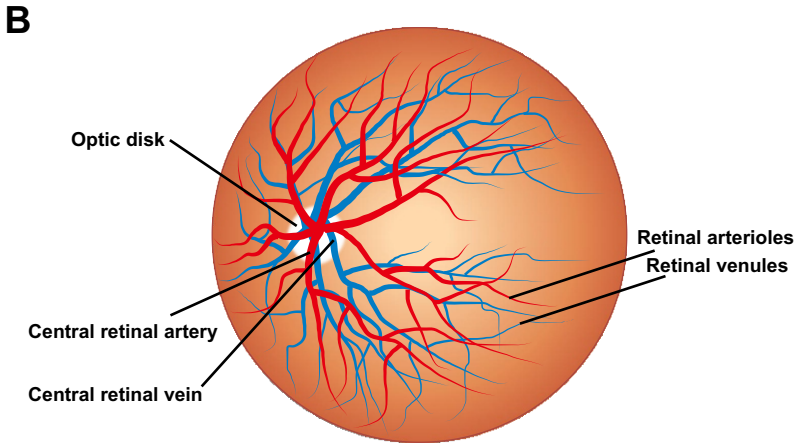
B
Optic disk
Retinal arterioles
Retinal venules
Central retinal artery
Central retinal vein

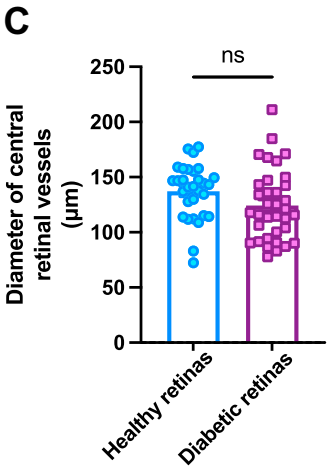
C
ns
Diameter of central retinal vessels (μm)
250
200
150
100
50
0
Healthy retinas
Diabetic retinas

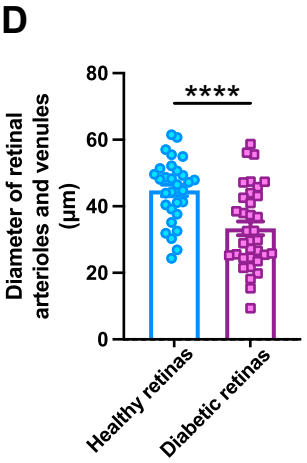
D
****
Diameter of retinal arterioles and venules (μm)
80
60
40
20
0
Healthy retinas
Diabetic retinas

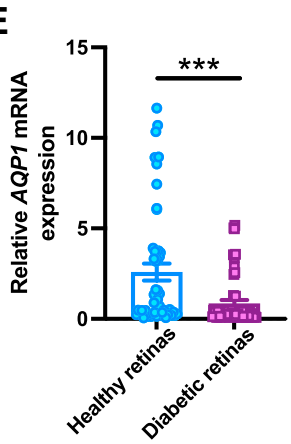
E
***
Relative AQP1 mRNA expression
15
10
5
0
Healthy retinas
Diabetic retinas

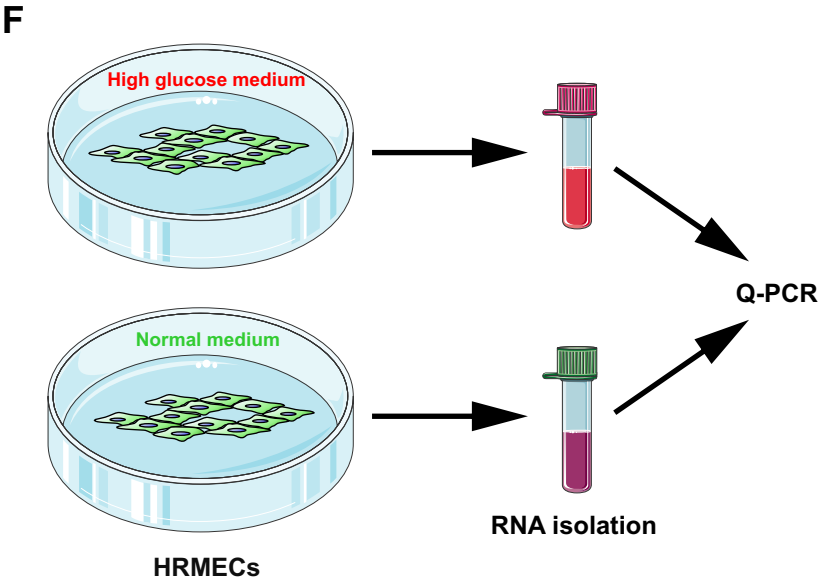
F
High glucose medium
Normal medium
HRMECs
RNA isolation
Q-PCR

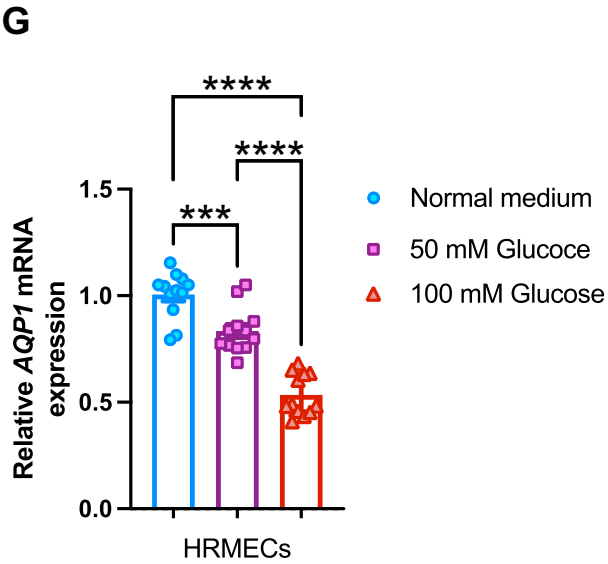
G
****
****
***
Relative AQP1 mRNA expression
1.5
1.0
0.5
0.0
HRMECs
Normal medium
50 mM Glucoce
100 mM Glucose

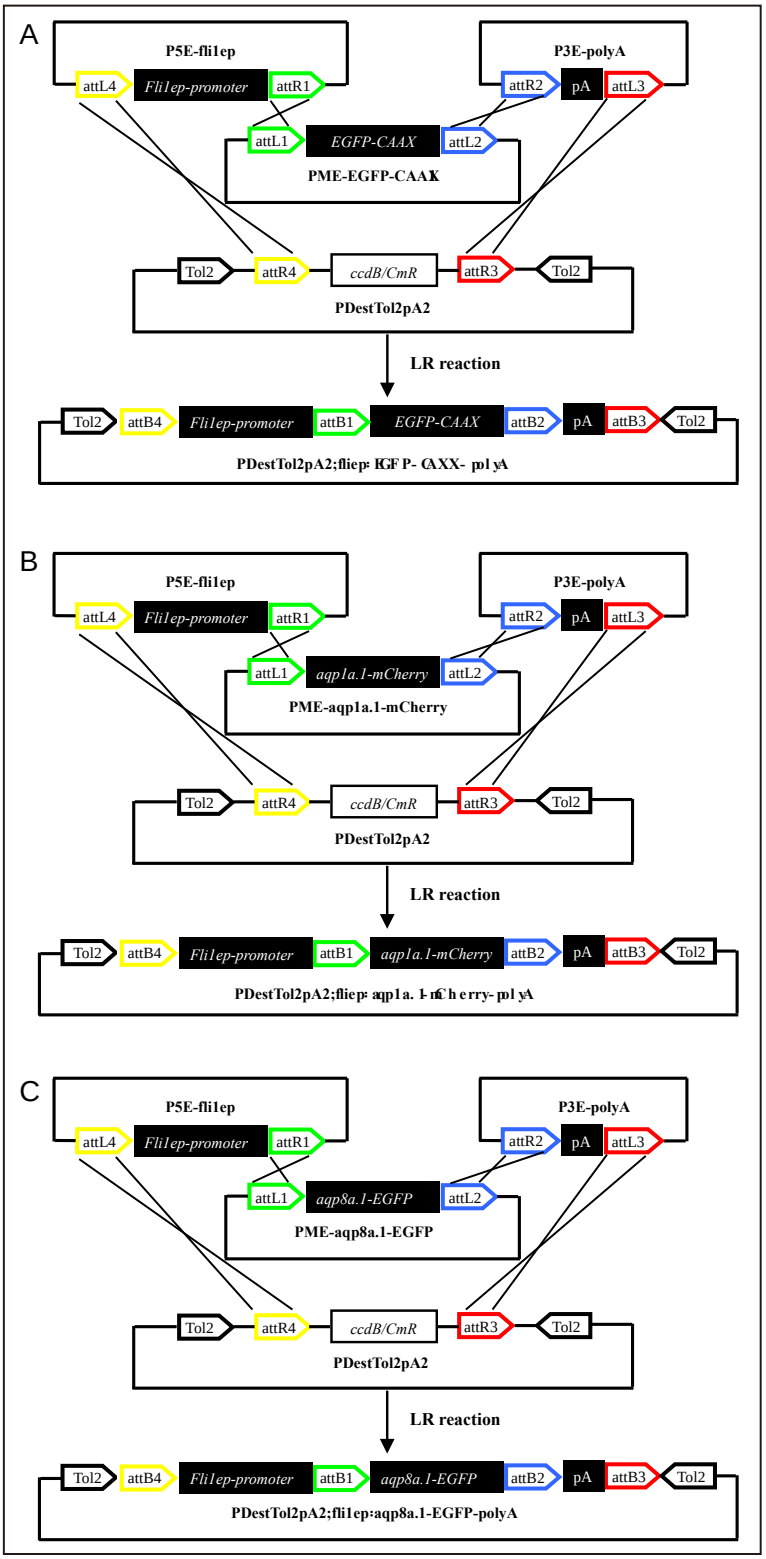

Supplementary Figure 1. The diagram for showing the constructs of three transgenic lines.

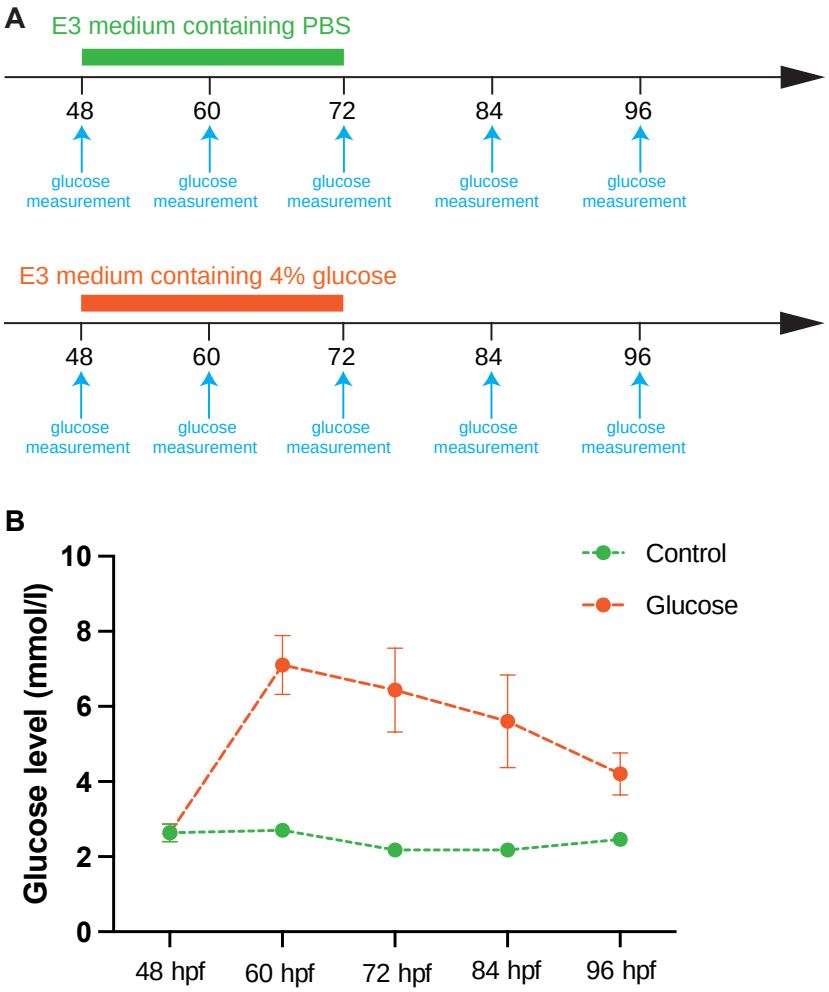

Supplementary Figure 2. The glucose treatment of zebrafish embryo. A. The time line of glucose treatment of zebrafish embryos. B. The glucose level of body fluid of zebrafish embryos.

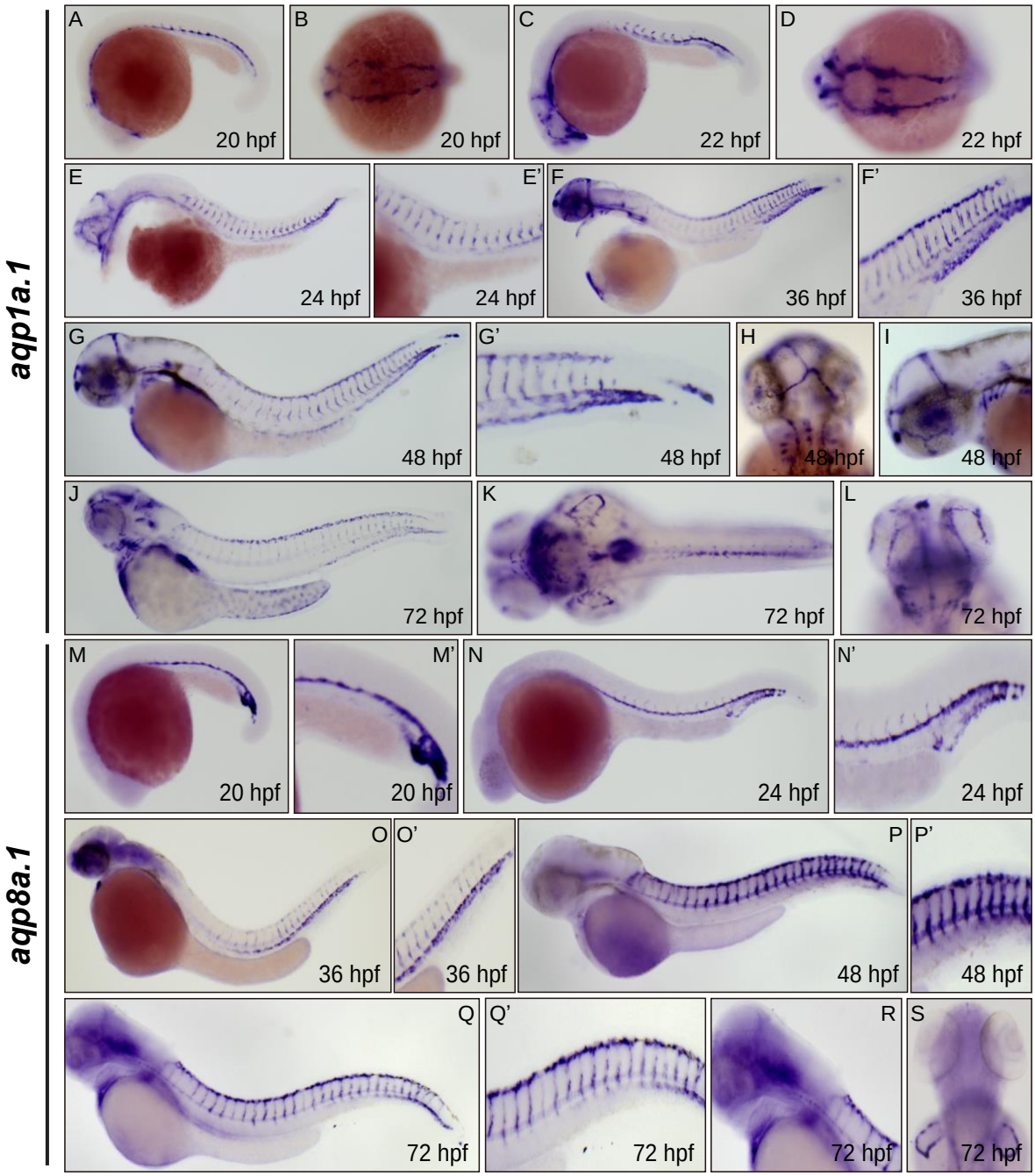

Supplementary Figure 3. WISH analysis of *aqp1a.1* and *aqp8a.1*. A-L. The *aqp1a.1* expression in 20 hpf, 22 hpf, 24 hpf, 36 hpf, 48 hpf and 72 hpf embryos. M-S. The *aqp8a.1* expression in 20 hpf, 24 hpf, 36 hpf, 48 hpf and 72 hpf embryos.

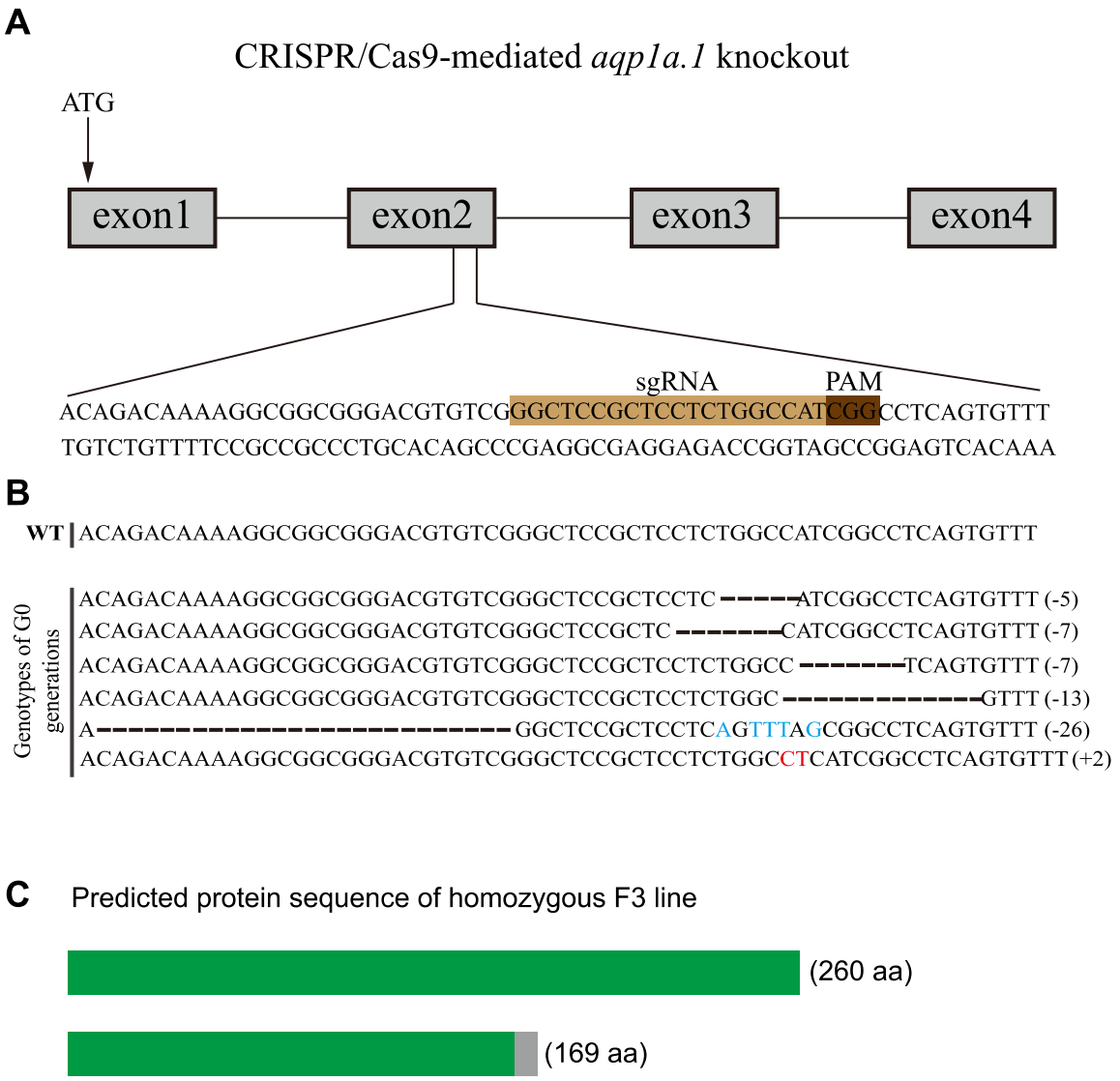

Supplementary Figure 4. Generation of zebrafish *aqp1a.1* knockout using CRISPR/Cas9. A. Schematic diagram showing gRNA targeting site on the second exon of *aqp1a.1* gene. Starting codon (ATG) site is indicated by arrow. B. Genotypes of G0 generations. Numbers in the brackets show the number of nucleotides were deleted (−) or inserted (+). Inserted nucleotide is in red. WT, wild-type. C. Schematic diagram showing the predicted proteins encoded by the two homozygous F3 line. The mutants are reading frameshift mutations that result in truncated proteins. The gray rectangles indicate the wrong coded amino acid sequences.

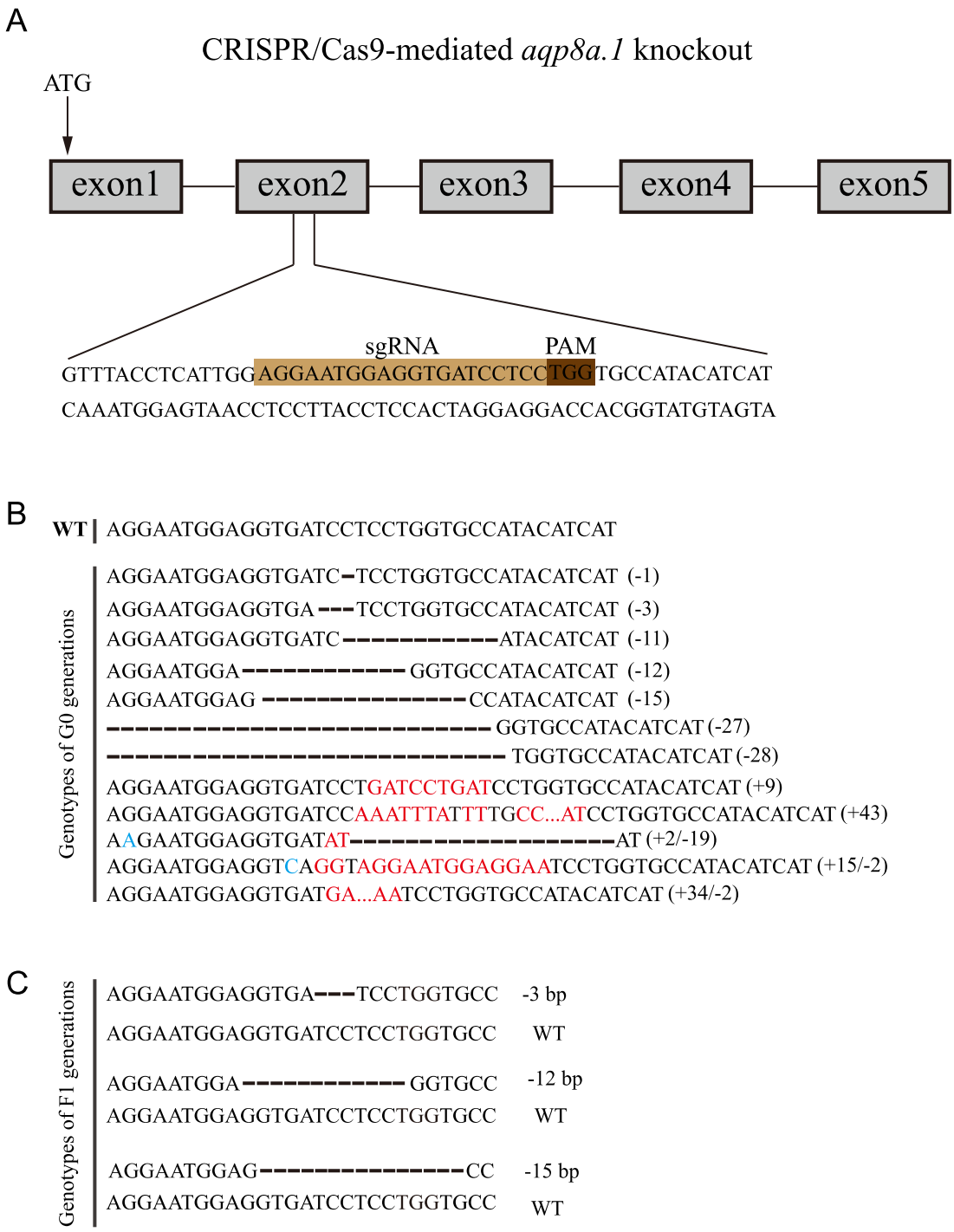

Supplementary Figure 5. Generation of zebrafish *aqp8a.1* knockout using CRISPR/Cas9. A. Schematic diagram showing gRNA targeting site on the second exon of *aqp8a.1* gene. Starting codon (ATG) site is indicated by arrow. B. Genotypes of G0 generations. Numbers in the brackets show the number of nucleotides were deleted (−) or inserted (+). Inserted nucleotide is in red. C. Genotypes of F1 generations.

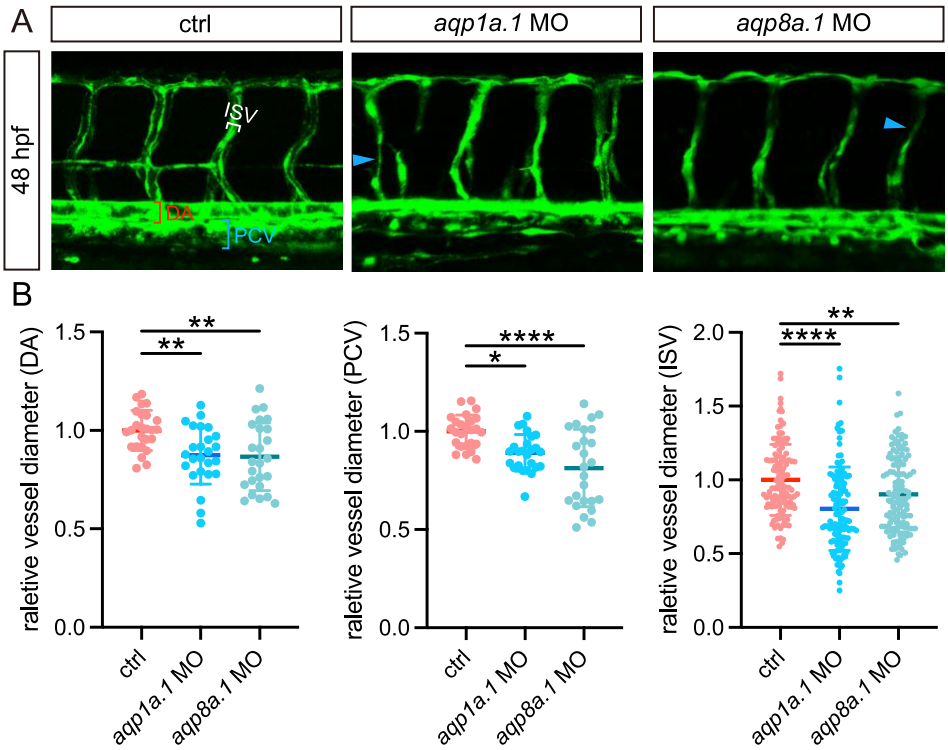

Supplementary Figure 6. Knockdown of EC-enriched aquaporins (*aqp1a.1* or *aqp8a.1*) leads to defective vascular lumenization in zebrafish. A, Confocal images of ISV phenotypes in 48-hpf *Tg(kdrl:EGFP)* control embryos and *aqp1a.1*-knockdown and *aqp8a.1*- knockdown embryos. Red and blue square brackets indicate artery and vein, respectively. Blue arrowheads indicate the narrowed ISVs. **B,** Quantification of the diameters of ISV, DA and PCV. Data are shown as mean ± s.e.m. One-way ANOVA analysis is applied. *, $p<0.05$. **, $p < 0.01$. ****, $p < 0.0001$.

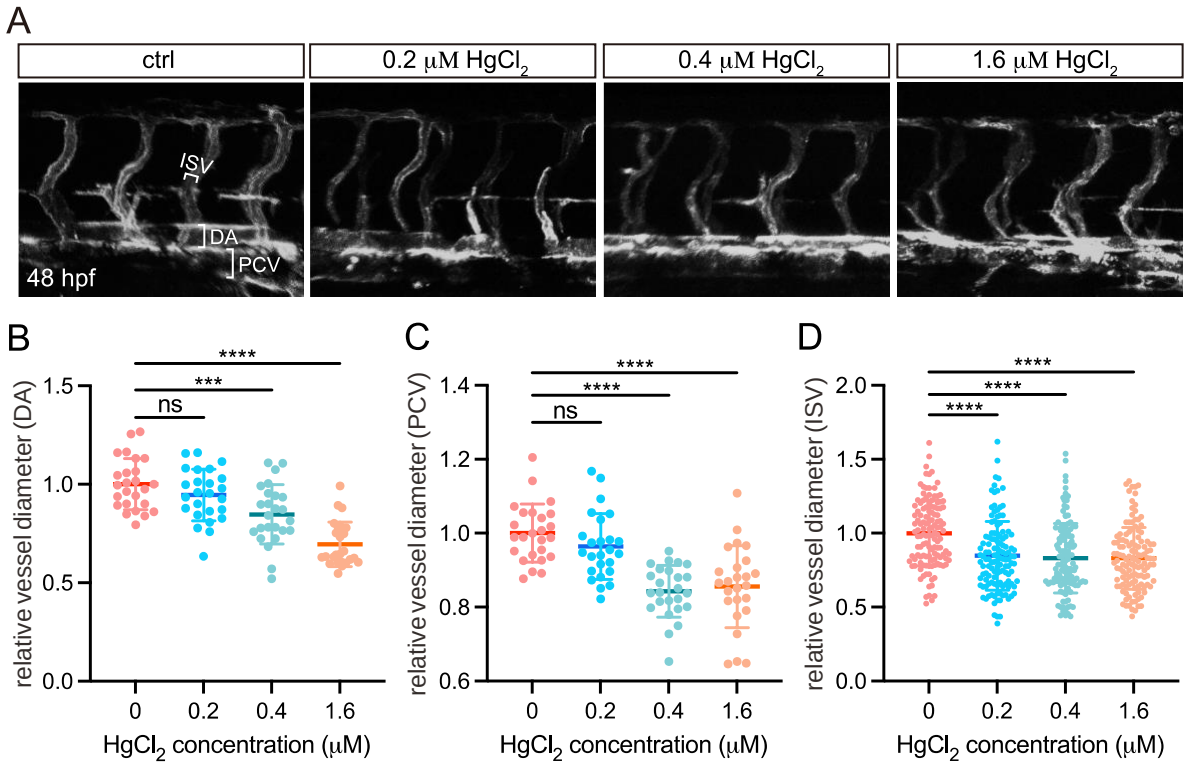

Supplementary Figure 7. $HgCl_2$ treatment impairs blood vessel lumenization. A, Representative confocal images of ISV phenotypes in 48-hpf *Tg(kdrl:ras-mCherry)* upon HgCl2 treatment. **B-D,** Quantification of the diameters of ISV, DA and PCV. Data are shown as mean ± s.e.m. One-way ANOVA analysis is applied. ns, not significant. ***, $p < 0.001$. ****, $p < 0.0001$.

Supplementary Table S1. Primer list

Primers for ISH probe synthesis		
	Left primer	Right primer
aqp1a.1	5’-CCCAGACCAGGAGATCAAGG-3’	5’-CGACCCAGTAGACCCAGTA-3’
aqp8a.1	5’-CTGCCCTTCTTCGAGCACTA-3’	5’-ATTTGCCGTCACAGTGAGTC-3’
Primers for RT-PCR		
	Left primer	Right primer
AQP1(Human)	5’-CCTCTCTGTAGCCCTTGGAC-3’	5’-GGCCAGGATGAAGTCGTAGA-3’
aqp1a.1(Zebrafish)	5’-CCCAGACCAGGAGATCAAGG-3’	5’-CGACCCAGTAGACCCAGTA-3’
aqp8a.1(Zebrafish)	5’-CTGCCCTTCTTCGAGCACTA-3’	5’-ATTTGCCGTCACAGTGAGTC-3’
sgRNA sequence		
aqp1a.1 sgRNA	5’-GGCTCCGCTCCTCTGGCCAT-3’	
aqp8a.1 sgRNA	5’-AGGAATGGAGGTGATCCTCC-3’	
Primers for sgRNA synthesis		
	Left primer	Right primer
aqp1a.1 sgRNA	5’-TGATACAAGTAGCATTCTGTGTCG-3’	5’-TGAGCATTCTCTAGCTGCA-3’
aqp8a.1 sgRNA	5’-CTATTCCTATTAGACCAAAGT-3’	5’-TGATGTGACCTGGAATC-3’
Morpholino (MO) sequence		
aqp1a.1 splicing MO	5’-GTGTGAATGCTGATTACTCACGGCT-3’	
aqp8a.1 splicing MO	5’-ACCACCACTGGAAAACAACAAGTGT-3’	